12-2021

Characteristics Analysis of Electrochemical Impedance Spectroscopy (Eis) for Different Electrode Patterns

Shanzida Kabir
The University of Texas Rio Grande Valley

CHARACTERISTICS ANALYSIS OF ELECTROCHEMICAL IMPEDANCE SPECTROSCOPY (EIS) FOR DIFFERENT ELECTRODE PATTERNS

A Thesis

by

SHANZIDA KABIR

Submitted in Partial Fulfillment of the

Requirements for the Degree of

MASTER OF SCIENCE IN ENGINEERING

Major Subject: Electrical Engineering

The University of Texas Rio Grande Valley

December 2021

CHARACTERISTICS ANALYSIS OF ELECTROCHEMICAL IMPEDANCE SPECTROSCOPY (EIS) FOR DIFFERENT ELECTRODE PATTERNS

A Thesis
by
SHANZIDA KABIR

COMMITTEE MEMBERS

Dr. Nazmul Islam
Chair of Committee

Dr. Hasina Huq
Committee Member

Dr. Paul Choi
Committee Member

December 2021

ABSTRACT

Kabir, Shanzida, Characteristics analysis of Electrochemical Impedance Spectroscopy (EIS) for different Electrode patterns. Master of Science in Engineering (MSE), December 2021, 76 pp., 6 tables, 43 figures, references, 47 titles.

Electrochemical impedance spectroscopy (EIS) is a rapidly developing technique used in characterizing materials and interfaces. Using equivalent circuits as models can determine the electrical properties of heterogeneous systems like membranes or electrolytes. Different electrochemical processes like the electron transfer rate of a specific reaction or the capacitive behavior of the system, or even the diffusion-limited response can coincide. EIS is applicable to determine different electrochemical processes that can happen simultaneously. The purpose of this research is to find the optimal operating range for other AC electrokinetic mechanisms. Analysis of EIS can be helpful in both fundamental examinations of electrokinetic transport of the micro or nano interface and even in the practical applications of biomolecular as a sensor or detector for integrated lab-on-a-chip devices. Both the micro-PIV and EIS experiments were done to verify the data validity of the microfluidics mixers.

DEDICATION

This journey cannot even start without one person, and that is my mother. She believes me when I can not even believe myself. She taught me not to be trapped in someone's else dream and inspired me to have my own vision. Also love for my father and brother, the two pillars who constantly teach me to fight against odds. Lastly, Thank you to all those well-wishers who were there through thick and thin.

ACKNOWLEDGMENTS

I would first like to thank my advisor Dr. Nazmul Islam, for his guidance and directions throughout the time of my degree. He always supports me in my work and gives instructions for my work and studies. He consistently directed me, urged me to work better in my research helped me whenever needed.

I would also like to acknowledge Dr. Hasina Huq and Dr. Paul Choi for being the committee members of this thesis, and I am gratefully indebted to their precious inputs on this thesis.

Finally, I would like to thank Salman Parvezand and KIM Iqbal for guiding me in my early days and Hector Zepeda for working and helping me during these whole time for many experiments. This can not be possible to accomplice with all of their help.

TABLE OF CONTENTS

Page

LIST OF TABLES

Page

LIST OF FIGURES

Page

CHAPTER I

INTRODUCTION

1.1 Overview of Lab-On-a-Chip (LOC) and Microfluidics

The application of laboratory-on-a-chip or lab-on-a-chip (LOC) devices is increasing rapidly because of its uses in molecular biology, proteomics, cell biology, and chemistry. It is a miniaturized device that can make biochemical analysis detection or DNA sequencing, or other complex human diagnostics into a single chip. Enhancing the time and cost is one of the main concerns in the field of LOC, which is also called micro total analysis system (μ-TAS). Conventional methods of bioparticle detection take a long time to complete, for which application of this LOC technology can be an effective way in the field of the diagnostic process. Microchannels are mainly used for microfluidics analysis which is often challenging and makes it hard to use generally. Microfluidic technologies used in LOC devices allow to manufacture of millions of microchannels, and these can measure the small amount of fluids on a single chip that fits in hand. For small size, high precision and sensitivity, easy maintenance, and less time consumption, this area of research is flourishing day by day.

In the near future, LOC devices, with their ability to perform a complete diagnosis of a patient during the time of consultation, can change our way of practicing medicine. A short time and accurate diagnosis with the help of LOC can significantly reduce antibiotic resistance, which is currently one of the biggest challenges of the decade. In the current costly medical era, it can

perform diagnosis at low cost, which can help increase the availability of medication and increase the rate of detecting illnesses at an earlier stage and treating them as soon as possible.

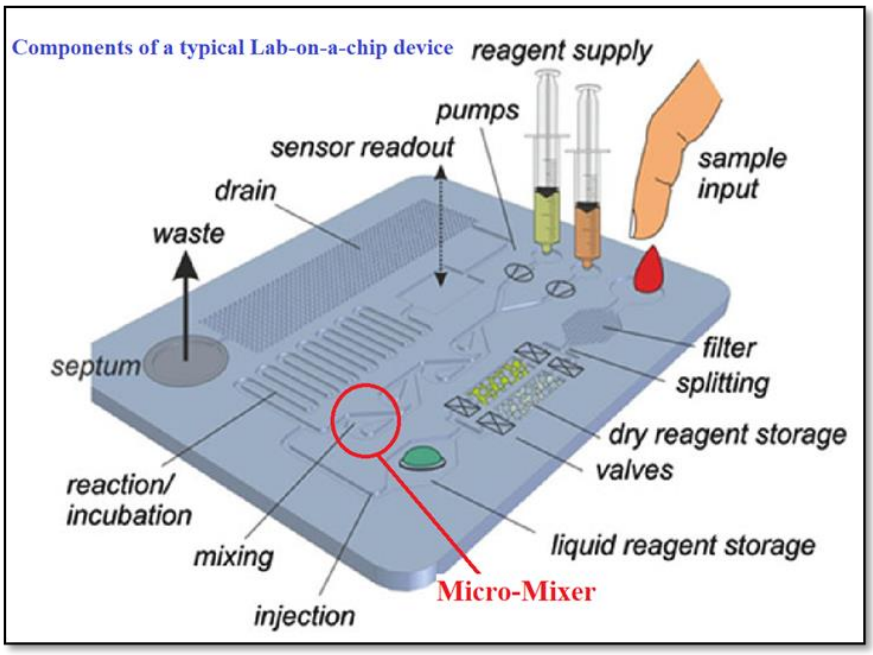

Figure 1.1: A general LOC device where multiple microfluidics techniques are applied on a single device [Castillo-Leon et al.]

One of the main problems of microchannels is manipulating microfluid flow as in standard operating conditions; most of these channels are laminar. The spontaneous fluctuations of velocity that tend to homogenize fluids in turbulent flow are missing, and molecular diffusion over the tracks is slow.

Manipulation or mixing in low Reynolds number is vital for most of the LOC applications for which AC Electrokinetic (ACEK) techniques can play a pivotal role. Figure 1 shows a typical LOC device that has different operations in a single microfluidics device.

1.2 AC Electrokinetic (ACEK)

AC Electrokinetic (ACEK) is one of the developing research areas due to its application in different fields of microfluidics. Electrokinetic forces can be differentiated into two main sectors: AC Electrokinetic (ACEK) and DC Electrokinetic (DCEK). ACEK has some upper hand over traditional EK or DCEK for electrochemical reaction or low ionic strength fluids limitation. Fundamentally, microfluid or particle motions are prompted by EK within a microchannel by an exciting electric field. The adequately high electric field strength can be achieved by scaling down the devices with relatively low voltage for EK techniques. Usually, EK devices involve no moving parts, and therefore they are simple and reliable [J. Wu]. ACEK is applied more for some of its advantages, like the low operating voltage, non-uniform streamlines, which can be used in mixing fluids and minimizing electrolysis and chemical reactions due to the application of low voltages [M.lian].ACEK mainly includes three primary mechanisms, which are Dielectrophoresis (DEP), AC Electroosmosis (ACEO), and AC Electrothermal (ACET). These techniques are described in detail here.

1.2.1 Dielectrophoresis (DEP)

Dielectrophoresis or DEP occurs when a particle is subjected to a non-uniform external electric field, and it experiences a net force and proceeds in the direction of either higher electric field strength or lower electric field strength for its polarity difference between the particle and the surrounding medium.

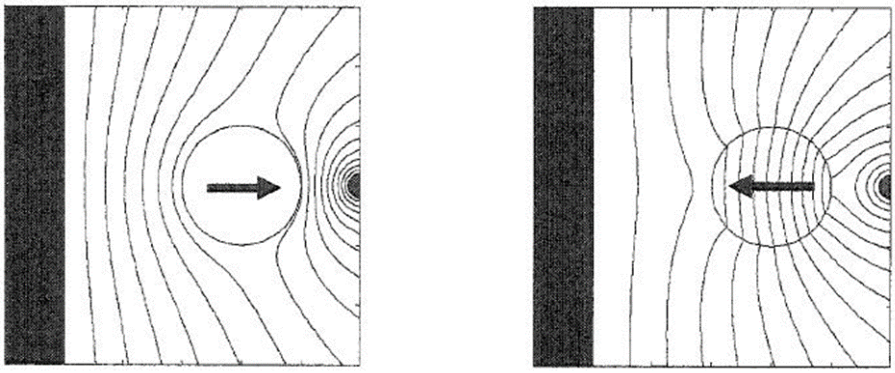

Figure 1.2: (left side) Positive DEP (right side) Negative DEP where the rectangular black areas represent the electrodes, and the arrows show the direction of DEP.

It is called positive DEP if a suspended particle has polarizability higher than the medium, and the DEP force will push the particle toward regions of the higher electric field. On the contrary, if the medium has higher polarizability than the suspended particle and the particle is driven toward regions of low field strength which causes negative DEP. The velocity of a spherical particle that is experiencing DEP will be,

$$u_{DEP} = \frac{a^2\,\varepsilon_m}{6\eta}\,Re\left[\frac{\widetilde{\varepsilon_p}-\widetilde{\varepsilon_m}}{\widetilde{\varepsilon_p}+2\widetilde{\varepsilon_m}}\right]\nabla|E|^2$$

$$or, u_{DEP} = \frac{a^2\,\varepsilon_m}{6\eta}\,Re[f_{CM}]\nabla|E|^2 \qquad (1.1)$$

Where $\widetilde{\varepsilon_p}, \widetilde{\varepsilon_m}$ are the complex permittivity of the particle and the medium, respectively, a is the diameter of the particle, η is the fluid viscosity. Clausius-Mossoti factor (f_{CM}) is used in the equation to indicate whether the particle manifests negative or positive DEP, which is determined by the difference of the dielectric properties of the particles and the surrounding medium.

In the manipulation of the particles like DNA, protein molecules, virus, bacteria, plant and animal cells, and inorganic particles, DEP can play an effective role [R. Peting].

1.2.2 AC Electroosmosis (ACEO)

By applying AC electric field, microelectrodes can induce AC voltages which can cause microfluidics flow for the charges at the electrode-electrolyte interface. The phenomenon which caused induced charges in the electrical double layer (EDL) is called AC Electroosmosis (ACEO). Due to the application of a small amount of AC signal over the electrodes, the surface becomes capacitively charged, which later forms counter-ion accumulation. The general expression of ACEO fluid velocity is given by,

$$u_{ACEO} = -\left(\frac{\varepsilon_m}{\eta}\right).\Delta\xi.\,E_t \tag{1.2}$$

Here ε_m and η are the permittivity and viscosity of the medium respectively and the electric field parallel to the solid surface expressed by E_t. Voltage drops over the charged double layer are denoted as $\Delta\xi$ and proportional to the induced charge density.

$$Q \sim \frac{\varepsilon}{\lambda_D}.\Delta\xi \tag{1.3}$$

The fluid motion in bulk can be solved using the Navier–Stokes equation with the electro-osmotic velocity as the boundary conditions. In the following figure 1.3, the electrodes are positioned in parallel in the conductive electrolyte. In figure 1.3(a), the double layer is created like a DCEO on the electrode surface. Due to finite thickness, an electric field line is not common in the double layer. That is why, with or against an electric field that is tangential to the electrode surface, the counter-ion migrates. In the figure1.3(b), the sign of the surface charge

becomes reversed from the previous one and this, in turn, produces fluid movement for the fluid viscosity.

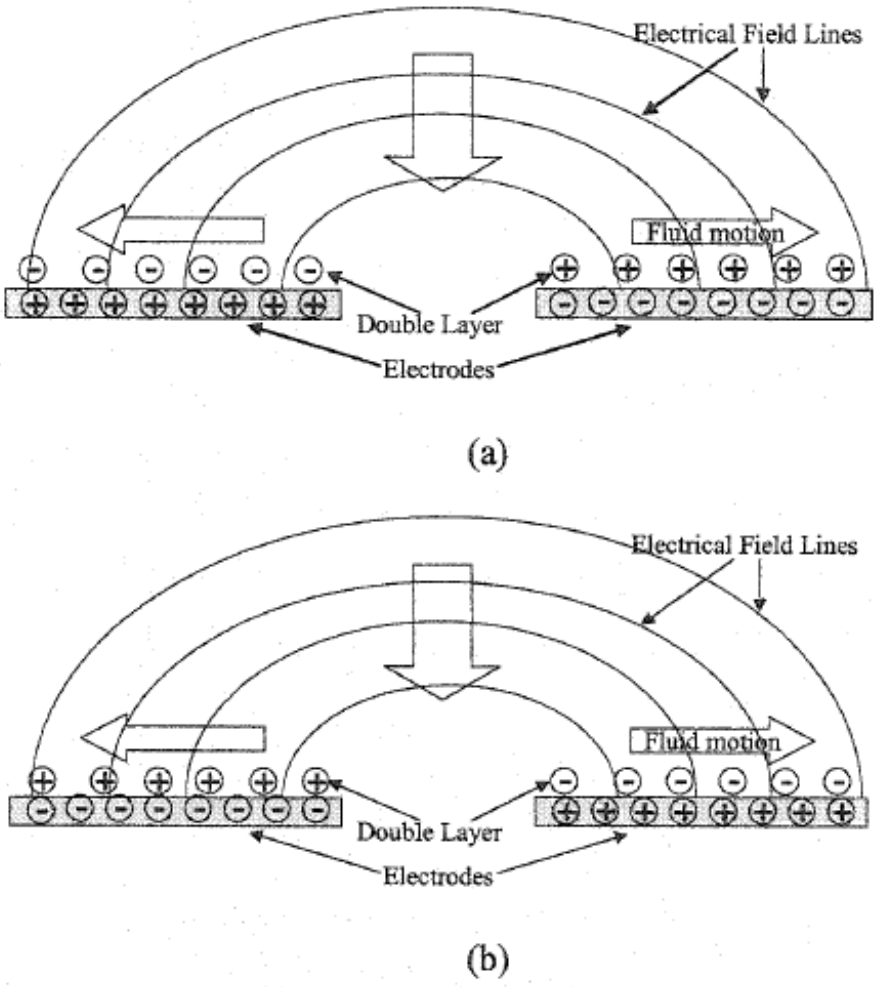

Figure 1.3: Schematic diagram of ACEO shows the counter-ion migration

Steady fluid motion is generated due to the tangential electrical field changing its direction with EDL charges instead of oscillatory flows. The EDL changes its polarity accordingly for the supply of AC signals. With the proper arrangement of electrodes, it is not hard to get synchronized tangential and normal electric fields for which many researchers

propose many designs to obtain a better outcome. Two of the familiar and widely used electrode arrangements are "side by side" [ju 4,5] and "face to face" electrode pairs[wu18, 19]. A side view of the side-by-side electrode pair is shown in figure 1.4, where it also reveals the electric field distribution through the lines.

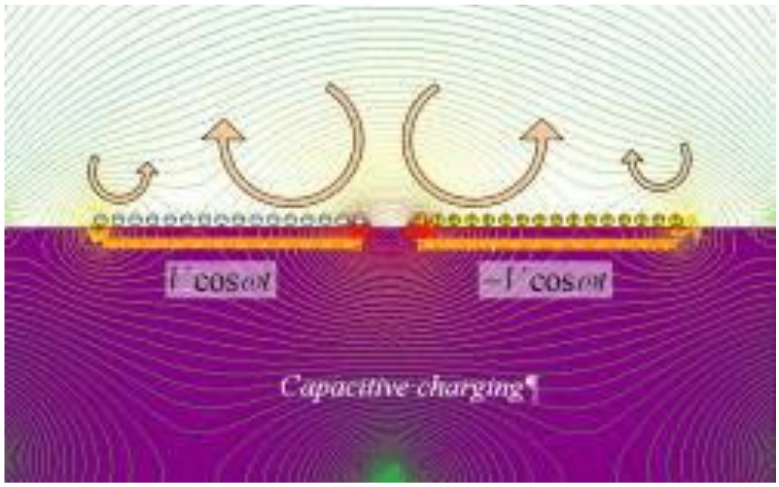

Figure 1.4: AC electro-osmotic flow originated by side by side electrode arrangement

From the figure, we can demonstrate that even in one electrode area, the tangential component of the specific electric field changes direction. That is why four counter-rotating vortices over the pair of electrodes are created. If L is the width of the electrode and a is the half of the electrode gap, we can express the positioning of the changing direction from the electrode's inner edge with $\sqrt{\frac{((L+a)^2+a^2)}{\sqrt{2}}}$ Equation. Fluid motion can be tracked down by mixing the fluids with specific particles that can move in directions consistent with capacitive charging. Besides manipulating the fluids particle, ACEO can be useful to exert a drag force through the fluid movement. Consequently, the ACEO technique is remarkably functional for manipulating particles from one place to another as well as fluids for their size-independent nature.

1.2.2 AC Electrothermal (ACET) effect

ACEO mechanism mainly depends on the EDL system, which is disrupted due to the high conductivity. For this reason, ACEO application is bound to the low ionic strength or low conductivity fluids like DI water. AC Electrothermal (ACET) effect is very effective in such high conductivity fluids and shows plateaus in force in the wide range of frequency.

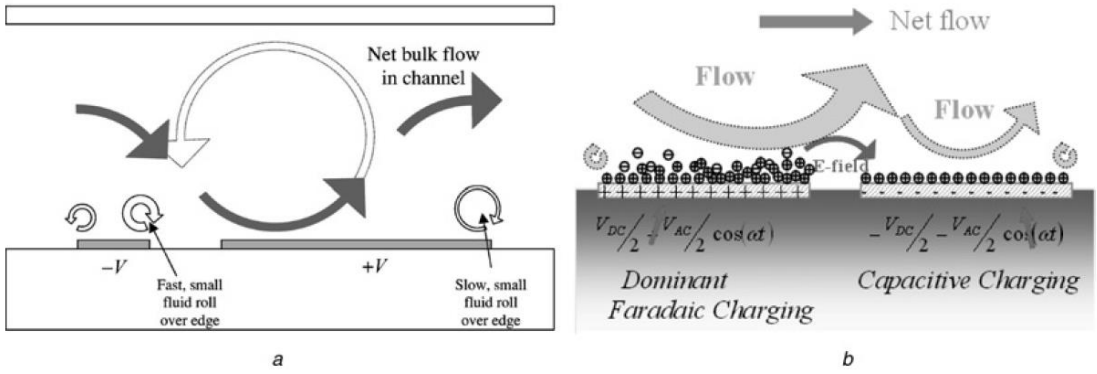

Figure 1.5: Electric field distribution [J. Wu et al.]

ACET force and velocity are firmer and more effectual in different frequencies compared to other ACEK technologies. It is the most effective electrokinetic application for most electrolytes, which have a high conductivity range (more than 0.7S/m). The temperature gradient of the fluid leads to gradients in the electrical substances (like conductivity or permittivity) of the fluids and induces free charge density. The free charges move due to an electric force that arises from the non-uniform electric field. Therefore, the surrounding fluid is also dragged for shear stress into the movement, creating microflow [A. Salari et al.].

$$k\nabla^2 T = -\sigma\langle E^2\rangle \tag{1.4}$$

Here, k and σ are the thermal conductivity and electrical conductivity respectively. T is the temperature which later leads to temperature gradient ∇T in the fluid and will produce a spatial gradient in fluid conductivity and permittivity by,

$$\nabla \varepsilon = \left(\frac{\partial \varepsilon}{\partial T}\right) \nabla T \qquad (1.5)$$

$$\nabla \sigma = \left(\frac{\partial \sigma}{\partial T}\right) \nabla T \qquad (1.6)$$

Laplace equation can be solved to encounter the electric field. If the free charge density is ρ_q in the bulk of the fluid, the equation will be,

$$\rho_q = \nabla . (\varepsilon E) = \nabla . E_0 + \varepsilon \nabla . E_1 \qquad (1.7)$$

This charge density in the AC electric field presence can develop microflow in the bulk of the fluid. The time-averaged electrothermal force $\langle f_e \rangle$ per unit volume can be evaluated by the following equation,

$$\langle f_e \rangle = -\frac{1}{2}\left[\left(\frac{\nabla \sigma}{\sigma} - \frac{\nabla \varepsilon}{\varepsilon}\right) . \overline{\mathrm{E}}_0 \frac{\varepsilon \bar{\mathbf{E}}_0}{1+(\omega\tau)^2} + \frac{1}{2} |\mathrm{E}_0|^2 \nabla \varepsilon\right] \qquad (1.8)$$

where ε, ω, and τ are electrical permittivity, angular frequency, and charge relaxation time, respectively.

CHAPTER II

LITERATURE REVIEW

2.1 Basic of Electrochemical Impedance Spectroscopy (EIS)

Electrochemical impedance spectroscopy (EIS) is a rapidly developing technique in microfluidics for characterizing materials and interfaces. By using equivalent circuits as models, it can determine the electrical properties of heterogeneous systems like membranes or fluids in a microfluidics chamber. For measuring Impedance spectroscopy, a small amount of perturbing sinusoidal signal was applied to the electrochemical microfluidic cell and measured the resulting current response.

2.1.1 Complex Impedance Values Representation

In EIS, the electrode or cell impedance is plotted against frequency. Electrochemical impedance is generally studied using a small amount of excitation signal. If a sinusoidal potential is applied, the response to this potential would be an AC signal. The values of the impedance are represented as a function of frequency to visualize the result [Bonora et al.]. The ratio of time-dependent sinusoidal voltage phasor and current phasor presents the impedance. In general, EIS data is expressed in terms of linear frequency.

For input frequency(ω) and time t, the magnitude of peak voltage is E_o, and the peak current is I_o. The phase shift between current and voltage is ∅. If E_t is the potential at time t and I_t is the response signal, then from Ohm's relation, we can get the impedance of the system,

$$Z = \frac{E_t}{I_t} = \frac{E_0 \sin \omega t}{I_0 \sin (\omega t + \emptyset)} = Z_0 \frac{\sin \omega t}{\sin (\omega t + \emptyset)} \quad (2.1)$$

Here, Z_0 is the magnitude and is ∅ the phase shift in the expression of impedance.

2.1.2. Steady State of Electrochemistry Systems

The fundamental theories of electrochemistry can be distinguished as either linear or non-linear. In the case of a potentiostat electrochemical cell system, though the input is in potential, the output is the current. So, changes that happen in the information don't affect the outcome linearly. As a result of non-linearity, the current response will contain harmonics of the excitation frequency. Analyzing EIS data takes a long time, and the system needs to be steady-state throughout the whole process. Working with a handmade channel and manually, it's often difficult to achieve perfect results in EIS. Also, the track can change throughout the process due to the solution interaction. That is why several data were collected of the same sample to achieve an absolute set of data.

2.2 Equivalent Electrical Circuit (EEC) Elements

The data that we got from EIS analysis is gained from fitting to an equivalent circuit model using common electrical elements like resistors, capacitors, and inductors. In such a setup, one resistance might constitute a conductive path, and a given resistor in the circuit might act for the bulk conductivity of the material or even the chemical step associated with an electrode reaction. Correspondingly, inductances and capacitances will stand in for an act like space-

charge polarization regions and with an adsorption and electro-crystallization procedure at an electrode. In these cases, the relationship between these elements can be expressed as impedance.

$$Z_{resistor}=R \tag{2.2}$$

$$Z_{capacitor}=\frac{1}{j\omega C} \tag{2.3}$$

$$Z_{inductor}= j\omega L \tag{2.4}$$

Where, $j=\sqrt{-1}$ and ω and f are the excitation frequency having the units of $rads^{-1}$ and Hz, respectively. C is the capacitance in F, and L is the inductance in H. For generating a specific equivalent circuit model for an EIS spectrum, impedance formulas are treated with the same procedure as resistors in circuit combinations. High precision measurements can be obtained by applying a small amplitude of externally defined potential.

The electrochemical modification that occurred at the interface of the electrode and electrolyte can be represented through an equivalent circuit by corresponding to the experimental data of impedance spectra.

The most used equivalent circuit is called the Randles and Ershler model for an electrochemical phenomenon. It includes the electrolyte solution's resistance R_s, the Warburg impedance(Z_w), which is used for the diffusion ions' from the electrode-electrolyte interface, electron transfer resistance R_{et} (if there was any redox probe in the liquids), and the double-layer capacitance C_{dl}[E. Katz et al.].

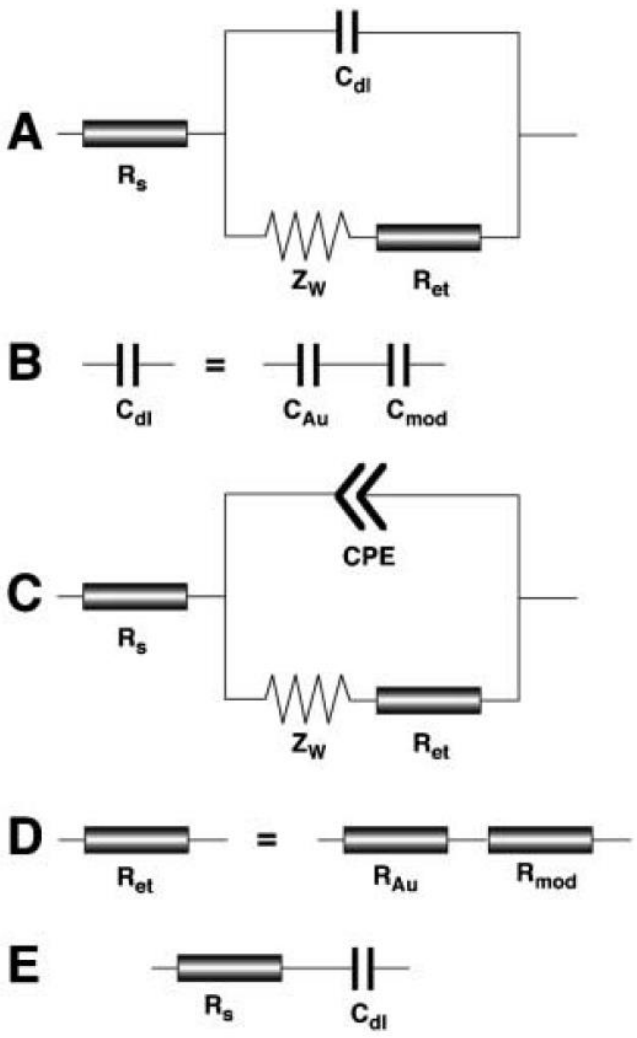

Figure 2.1: Randles Cell as an equivalent circuit for electrochemical impedance spectroscopy and equivalent circuit of other measurements of the electrochemical system

In figure 2.1(A), the circuit has two parallel elements, one of which represents the Faradaic process(Z_W+R_{et}), and the other one is the double layer charging method (C_{dl}) that comprises variable components C_{mod}. All current (I_f+I_c) pass through these elements are the contributions from the Faradaic process I_f and double layer charging I_c. As R_s (uncompensated resistance of the electrolyte solution)and Z_w (Warburg impedance) represent bulk properties of the fluids and diffusion features of the redox probe, they are not affected by the chemical

reaction that happened on the surface of the electrode. Furthermore, double-layer capacitance (C_{dl}) and electron transfer resistance(R_{et}), including variable component Rmod, mainly depend on dielectrics and insulating characteristics at the electrode and electrolyte interface. Therefore, the capacitance of the double layer relies on the dielectric permittivity institute into the double charged layer molecules, ε_{dl}.

$$C_{dl} = \frac{\varepsilon_{dl} A}{\delta} \tag{2.5}$$

In this equation $\varepsilon_{dl} = \varepsilon_o \varepsilon_{\rho}$. Where ε_o is the dielectric constant of the vacuum($8.85*10^{-12}$ F/m), and ε_ρ is the effective dielectric constant of the separating layer of ionic charge and the electrode surface. Depending on the roughness of the electrode surface, a general equivalent circuit with a constant phase element (CPE) is used. In that setup, the double layer capacitance C_{dl} can be depicted as a resultant of the unmodified electrode and a variable capacitance C_{mod}.

$$\frac{1}{C_{dl}} = \frac{1}{C_{unmod}} + \frac{1}{C_{mod}} \tag{2.6}$$

Occasionally, the constant phase element (CPE) is used in Randles and Ershler's models for the rough surface. When the electrode surface properties can be best described by a capacitive element that reflects the non-homogeneity of the layer, constant phase element (CPE) played a pivotal role to get a better insight.

$$\text{CPE} = A^{-1}(j\omega)^{-n} \tag{2.7}$$

This method is controlled by the parameter n, which is the number of transferred electrons per molecule of the redox probe. A is the area of the electrode surface. When n tends to zero, the co-efficient becomes equal to C_{dl}.

One of the prime parameters governing the EIS process is the applied frequency. EIS analyses in a specific range of frequencies which is important to define for a certain electrolyte or a system. When the frequency is lower than 1mHz, the value of impedance is normally determined by the DC conductivity of the electrolyte fluids, and thus the range is considered as the lower range. Again, when the frequency is higher than 100kHz, it is considered as a higher range, and in this range, the inductance of connecting wires and the electrical cell could contribute to the impedance spectra. In consequence, the range in between(10mHz to 100kHz) identifies analytically meaningful and is used to record the EIS data, which are largely controlled by interfacial properties of the modified electrode.

.

CHAPTER III

METHODOLOGY AND EXPERIMENTAL PARAMETRES

For manipulating micro or nano particles one of the major concerns for researchers is optimizing the overall cost and time of the whole process. In our research

3.1. Data Presentation and Explanation for EIS

Two main ways to visualize EIS are Nyquist and Bode plot. In our research, both of these plots describe the characteristics of the electrochemical system in their ways. Our studies analyzed both the Bode plot and Nyquist plot for different electrode arrangements named T-shaped electrodes (or orthogonal electrode), V-shaped electrodes, and array-shaped electrodes.

3.1.1 Bode Plot

In the Bode Plot, total impedance in logarithm and phase shift is plotted against the logarithm of the frequency response. Bode plot is more popular for its visible information in the graphs. In this, the dependency of the frequency is quite apparent and has less data lost. A capacitor with a parallel with a resistor is an important and common circuit for electrochemical impedance spectroscopy, which is perceptible in the bode plot as the top in the phase shift(φ). It is represented as the impedance(Z) and phase(φ) shift in the same plot against frequency. For comparison and analysis purposes, we showed them in different plots. Because of the very high value of the frequency and impedance, we have used a log scale for convenience.

$$|Z|\sqrt{Z_{RE}^2 + Z_{IM}^2} \tag{5}$$

$$\varphi = \tan^{-1}(\frac{Z_{IM}}{Z_{RE}}) \tag{6}$$

The magnitude is the vector quantity $|Z|$ impedance which consists of the real Z_{RE} and imaginary part Z_{IM}. The phase (φ) also consists of these real (Z_{RE}) and imaginary (Z_{IM}) part and the slope of the transformation area in between both asymptotic limits give the idea of the influence of the frequency dependence.

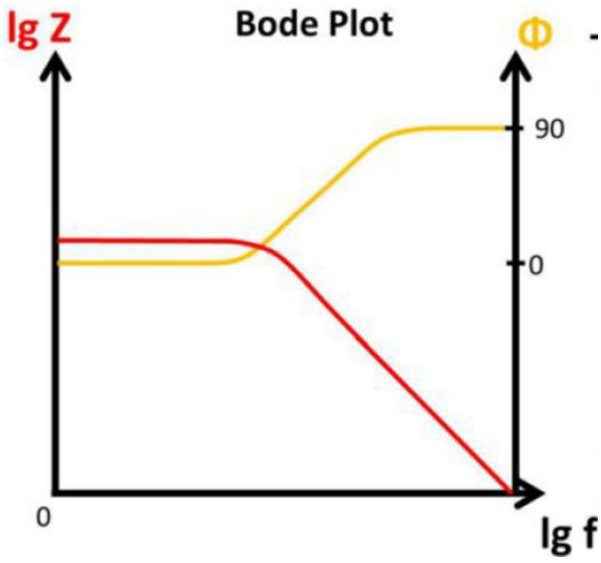

Figure 3.1: A general representation of Bode plot

As we got a large range of values for frequency(f) and impedance(Z), it is more efficient to plot them on a log scale so that it gets easier to examine the small values.

3.1.2 Nyquist Plot

A typical Faradaic impedance (capacitance and resistance function simultaneously at the surface of an electrode) spectrum, which is normally presented by a complex Nyquist plot,

includes a semicircle or some part of a semicircle. This mainly occurs because of the charge transfer resistance and the double-layer capacitance.

The data is collected from an actual equivalent circuit, and for each given frequency, the real part (Z' or Z_{RE}) and imaginary part (-Z" or Z_{IM}) are charted in the abscissa and the ordinate, respectively. Each graph can characterize the kinetic domination by an electrochemical charge deviation step at the interface of the electrodes and fluids surface. Generally, the left side indicates a higher frequency than the right side.

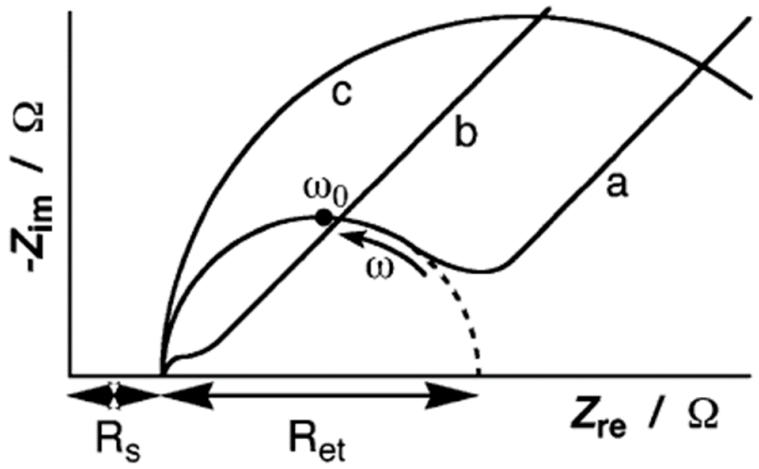

Figure 3.2: Schematic Faradaic impedance spectra presented in the form of a Nyquist plot

A stereotypical form of a Faradaic impedance spectrum is given in figure 3.1 where different kind of possibilities is presented and from which we can demonstrate different characteristics. In the figure 3.1 (a) a modified electrode is indicated where the impedance is controlled by diffusion of the redox probe (low frequencies) and by the interfacial electron transfer (high frequencies). So, the semicircle portion of this graph correlated to the electron transfer limited process and the straight after that indicate the characteristics of the lesser frequencies.

In figure 3.1 (b) a modified electrode designated where the impedance is mostly controlled by diffusion of the redox probe and in figure3.2(c) here the impedance is controlled by the interfacial electron transfer within the whole range of the frequencies that applied.Here, the dart shows the direction of the frequency increase. Resistance of the electrolyte solution, Rs, and electron transfer resistance, Ret, are shown with the dimensions.

If the overall impedance of an electrochemical cell is Z, then it consists of the combination of the resistance R_B and the impedance of the series capacitance C_B which can be expressed as:

$Z_{Re} = R_B$ and $Z_{Im} = \frac{1}{\omega C_B}$. The equivalent impedance of general Randles models can be expressed as follows:

$$Z_{Re}=R_{B=}\ R_{\Omega} + \frac{Rs}{A^2+B^2} \tag{3.1}$$

Where, $A=\frac{C_d}{C_s} + 1$ and $B=\omega R_s C_d$, Similarly

$$Z_{Im}=\frac{1}{\omega C_B} = \frac{(B^2/\omega C_d + A^2/\omega C_s)}{A^2+B^2} \tag{3.2}$$

In the case of low frequency when $\omega \rightarrow 0$ equation 3.1 and 3.2 can be express as follows:

$$Z_{Re}= R_{\Omega}+R_{ct}+\sigma\omega^{-1/2} \tag{3.3}$$

$$Z_{Im} = \sigma\omega^{-1/2} +2\sigma^2\ C_d \tag{3.4}$$

Eliminating ω from equations 3.3 and 3.4 we can get a linear equation of the impedance.

$$Z_{Im} = Z_{Re} - R_{\Omega} - R_{c\,t} + 2\sigma^2\ C_d \tag{3.5}$$

Therefore, this equation that the Nyquist plot (plot of Z_{Im} vs Z_{Re}) indicates a linear form and has a unit slope . In figure 3.3 this line intersect the real axis at $R_{\Omega}+R_{ct} -2\sigma^2\ C_d$.

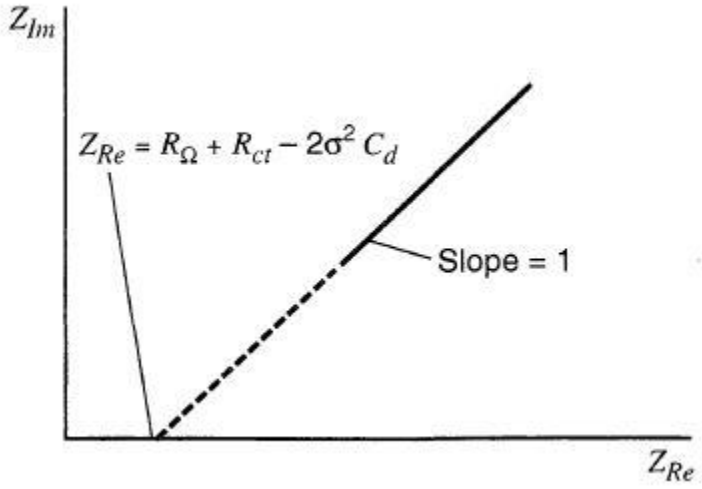

Figure 3.3: Nyquist plot of low frequencies.

At very high frequencies when $\omega \rightarrow \infty$ the Warburg impedance becomes insignificant and the total impedance of the cell **Z** becomes,

$$\mathbf{Z}=R_\Omega - j\left(\frac{R_{ct}}{R_{ct}C_d\omega - j}\right) \qquad (2.19)$$

The Real and Imaginary components of the equation 2.19 are as follows:

$$Z_{Re} = R_\Omega + \frac{R_{ct}}{1+\omega^2 C_d{}^2 R_{ct}{}^2} \qquad (2.20a)$$

$$Z_{Im} = \frac{\omega C_d R_{ct}{}^2}{1+\omega^2 C_d{}^2 R_{ct}{}^2} \qquad (2.20b)$$

Eliminating ω from equation 2.20a and 2.20b we can find,

$$\left(Z_{Re} - R_\Omega - \frac{R_{ct}}{2}\right)^2 + Z_{Im}{}^2 = \left(\frac{R_{ct}}{2}\right)^2 \qquad (2.21)$$

So, Z_{Im} vs Z_{Re} gives a circular plot which has a center at $Z_{Re}= R_{\Omega}+\frac{R_{ct}}{2}$, $Z_{Im}=0$ and having a radius of $\frac{R_{ct}}{2}$. Figure 2.7 depicts the result

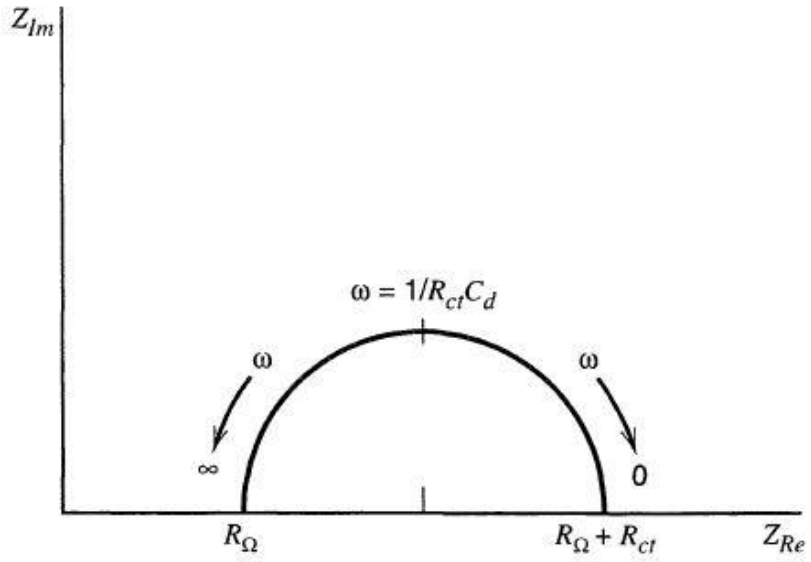

Figure 3. 4: Nyquist plot for high frequencies

3.1.3 EIS Data fitting

Electrochemical impedance spectroscopy (EIS) is a dynamic technique that gives information on the processes that occurred at the electrode-electrolyte interface. The data which get from EIS can be modeled with suitable electrical equivalent circuit which mostly known as data fitting. It used elements like resistors (R), capacitors (C), inductors (L), and ad-hoc elements like constant phase element (CPE) and Warburg (W). Each of the elements here is characterized by an impedance Z (Ω) described by a complex function with one or more parameters free to change during the fit. In the software NOVA 2.1 use a nonlinear least square regression to fit the data with the function from the equivalent circuit, using the Levenberg–Marquardt algorithm.

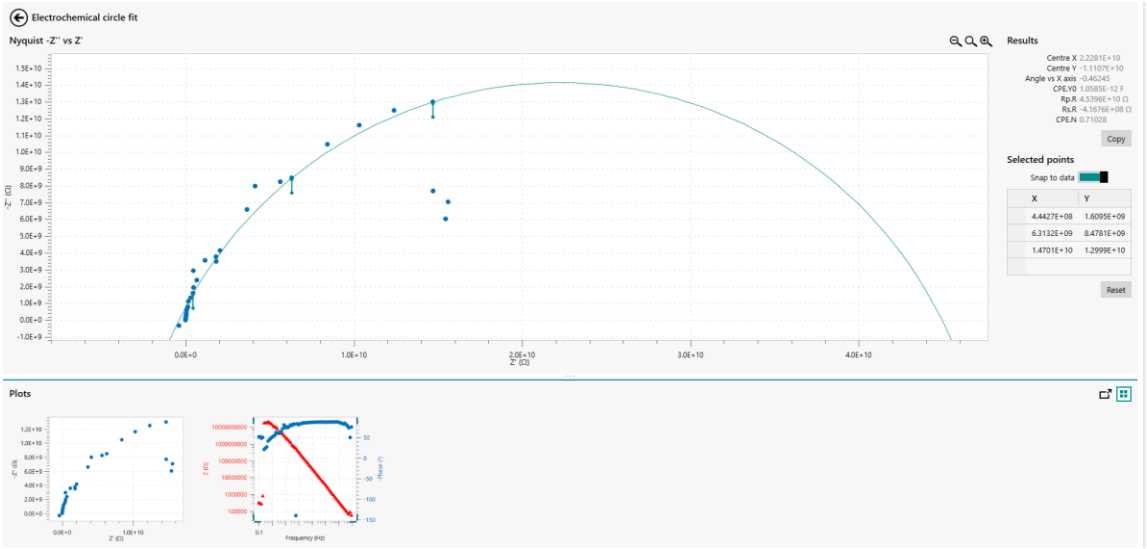

Figure 3.5: Selecting dots for preferable data setting from EIS data

A possible model to fit the data created by the software. It can be adjusted by adding elements and corrections if needed. Generally, it should include a resistance for the electrolyte, one resistance for the charge transfer, a capacitor (C) or a constant phase element (CPE) for the double layer, and a Warburg (W) for the semi-infinite diffusion of the ionic species through the diffusion layer.

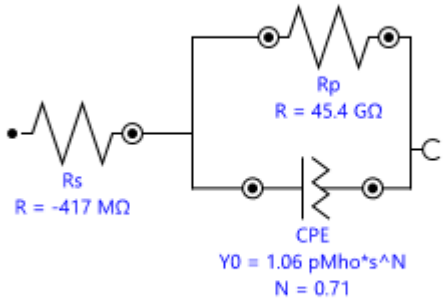

Figure 3.6: Representation of a simple Randles diagram from the EIS data fitting

CHAPTER IV

EQUIPMENT AND SOFTWARE TOOLS

For the experiments, Autolab potentiostat/galvanostat is used, and for EIS analysis for particle manipulation, we use Micro-Particle Image Velocimetry (μPIV) System. Besides these two leading equipment, we also need some software tools (like Solid works, NOVA 2.1, Insight 4G) to design and simulate and analyze the data. Furthermore, we also need some essential tools like a general microscope to measure or Polydimethylsiloxane (PDMS)and a glass slide for covering the microchannels.

4.1 Required Equipment for the experiments

The description of the equipment is mainly divided into two parts. One is the primary components like a whole set of Autolab potentiostat, μPIV system, and 3D printer. The later part mainly gives the idea of the subsidiary tools used in the experiments.

4.1.1 AutoLab Potentiostat/Galvanostat

A potentiostat that is used in most electroanalytical experiments is the electronic hardware required to control a three-electrode cell. It can also work with two working electrodes contained in an electrochemical cell. The instrument controls the cell current rather than the cell voltage as a galvanostat. AUTO LAB PGSTAT302N is used for this experiment, which is a

high-end, high current potentiostat with a compliance voltage of about 30V and a bandwidth of 1MHz, combined with the FRA32M module.

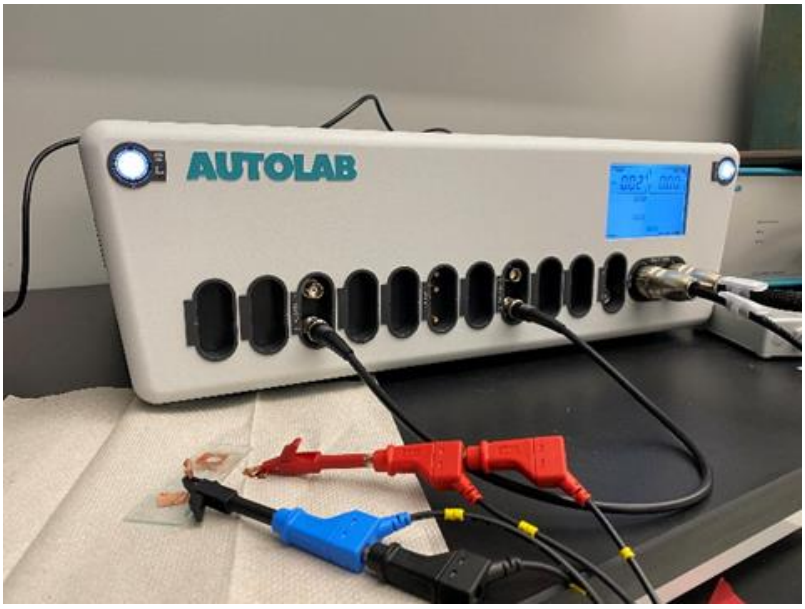

Figure 4.1: Set up of the T electrode in the Autolab potentiostat/galvanostat (AUTO LAB PGSTAT302N)

This potentiostat PGSTAT302N is the inheritor of the previous well-known model PGSTAT30. The highest range of current for this model is 2 A, the current range can be extended to 20 A with the addition of the BOOSTER20A, the current resolution is 30 fA at a current range of 10nA.

Figure 4.2: The current booster used with PGSTAT302N

The Booster 10A/20A module increases the maximum current of the PGSTAT302N to 10 Ampere to 20 Ampere. The compliance voltage of the system is 20 V in combination with the Booster10A. Some of the key tech features of this module aregiven below.

Table 4.1: Some key specifications of AUTO LAB PGSTAT302N

Key Specification	**Parameters (Unit)**
Electrode Connections	2,3, and 4
Potential Range	+/- 10V
Compliance Voltage	+/- 30V
Dimensions (W/H/D)	520mm/160mm/420 mm
Maximum Current	+/- 2A (20A with Booster20A)
Current Ranges	1 A to 10 nA in (100 pA with ECD module)
Potential Accuracy	+/- 0.2%
Potential Resolution	0.3µV(gain 1000)
Current Accuracy	+/- 0.2%
Current Resolution	0.0003%
Input Impedance	>10Tohm
Potentiostat Bandwidth	1 MHz
Computer Interface	USB
Control Software	NOVA 2.1
Weight of the instrument	18 kg

For the experiments the microchannel's electrodes are connected with the positive and negative parts of the potentiostat. In two-electrode mode, the counter electrode (CE) and reference electrode (RE) are connected together and considered as one connection, while the working electrode(WE) is connected to the other electrode. The current is normally measured between the two main channel of the counter electrode (CE) and the working electrode (WE).

4.1.2 Micro-Particle Image Velocimetry (μ-PIV) System

A typical Micro-Particle Image Velocimetry (μ-PIVor Micro-PIV) System consists of a sensitive scientific camera, synchronizer, a pulsed laser with proper beam coupling and guiding, an epifluorescence microscope which can be either single channel or stereo and a particular software for image acquisition, advanced analysis and intuitive visualization which contain reporting and export functionality. Micro-PIV systems are highly customizable. There are many options and equipment options that exist for the microscope, light source, seed particles, cameras, objective lenses, filter cubes, and more. In our lab the μ-PIV consists of the following items,

A) YAG70-15-QTL Laser power unit

B) YAG70-15-QTL Liquid light guide assembly

C) Laser pulse synchronizer

D) CCD camera

E) Nikon Eclipse LV150N Microscope

F) Insight 4G Data Acquisition, Analysis and Display package

G) Tecplot Focus Software

H) Function generator and

I) High-Voltage Amplifier

In a typical Micro-PIV an inverted microscope is used with fluorescent particles and a pulsed laser source for particle excitation. For the reflected light arrangement, a Micro-PIV System typically depends on narrow depth-of-field imaging which is common microscope optics to obtain results on the plane of interest. Emission of the laser and the image capturing device work concurrently tracing the movement of the fluorescent particle in the micro chamber.

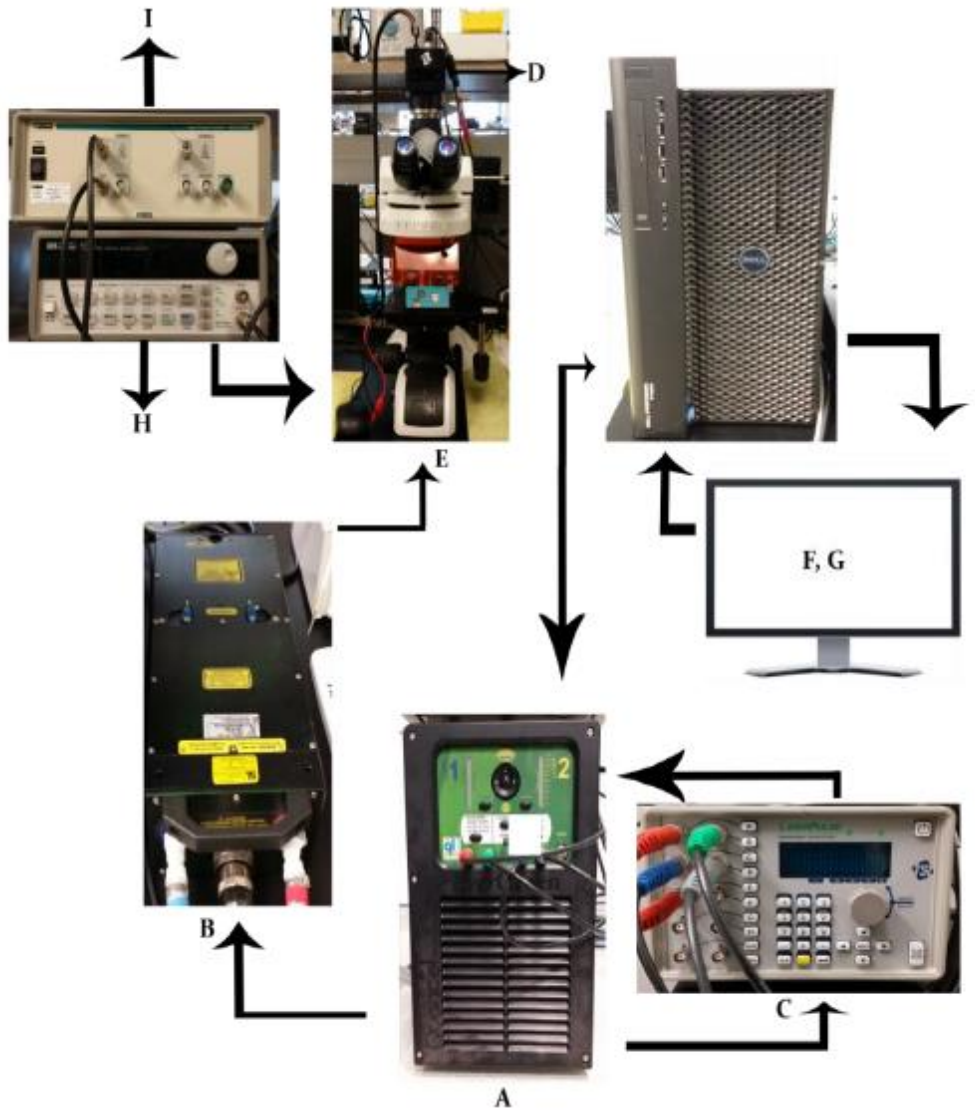

Figure 4.3: Different parts of the Micro-PIV System

In the conventional PIV system, it is not possible to observe the channel flow for its small dimension. Whereas, In the micro-PIV system it used the techniques of volume illumination where the light source and the observation field are introduced through identical optics. With this formula the focal plane proceeds down through the flow field to portray the entire volume.

4.1.3 Resin 3D printer

In today's world 3D printing continues to become cheaper and more accessible. Resin 3D printers have become a favorable choice for anyone interested in making highly detailed models that wouldn't be feasible using a filament-fed 3D printer or fused deposition modeling (FDM). This Masked Stereolithography (MSLA) resin 3D printers typically only have a single axis of motion, and this simple mechanical system means these machines can find at a cheap rate. In the experiment Elegoo Mars Pro MSLA UV Photocuring LCD 3D Printer is used.

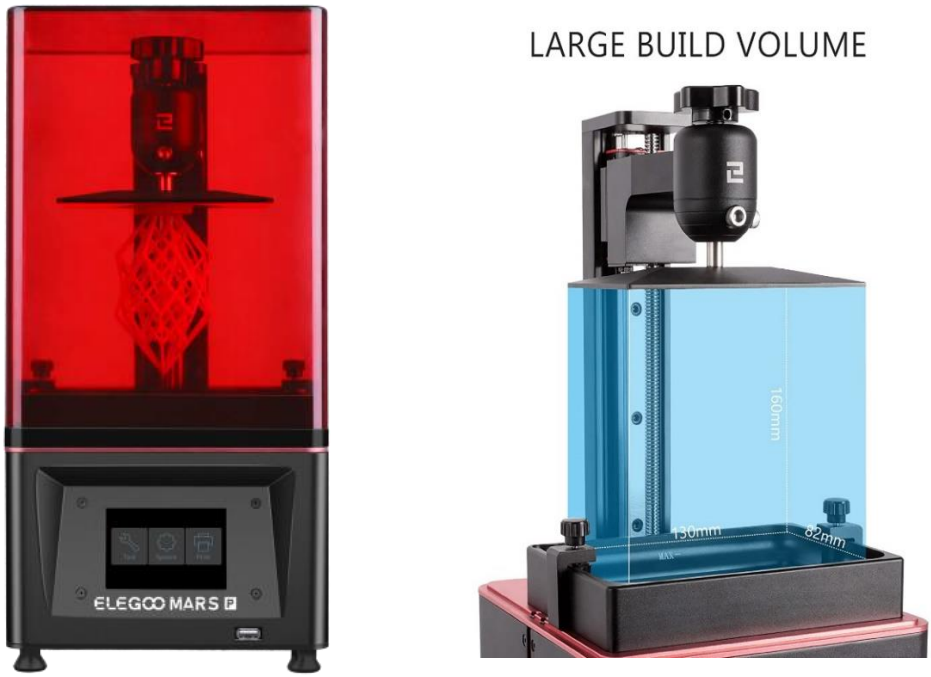

Figure 4.4: Elegoo Mars Pro Resin 3D printer

Table 4.2: Technical specification of Elegoo Mars Pro MSLA UV Photocuring LCD 3D Printer

Item weight	7.5 kg
Printer Dimensions(L/W/H)	7.87×7.87×16.14 in^3
Technology	LED Display Photocuring
Operation	3.5 Inch Touch Screen
Light source	UV Integrated Light (wavelength 405nm)
XY resolution	0.047mm (2560*1440)
Z-axis accuracy	0.00125mm
Layer Thickness	0.01-0.2mm
Printing Speed	22.5mm/h
Power Requirements	110-220V, 55/60Hz, 12 V, 5A, 60W
Dimensions(L/W/H)	20×20×41 cm^3
Build Volume(L/W/H)	12×6.8×15.5 cm^3
Slicer Software	Chitu Box
Printing Method	USB off-line printing

Mars 2 Pro has a 6.08-inch monochrome LCD of 2K HD 2560 × 1620 resolution, single-layer exposure, which takes 1.5 -2 seconds. The maximum printing speed is 50mm/h and the screen service life can be up to 2000h, which is more durable than an ordinary screen. The MSLA process uses a masking LCD to selectively occlude the UV light on a pixel-by-pixel basis. Thus this process allows these printers to create models that have a resolution of down to .035mm on the XY axes.

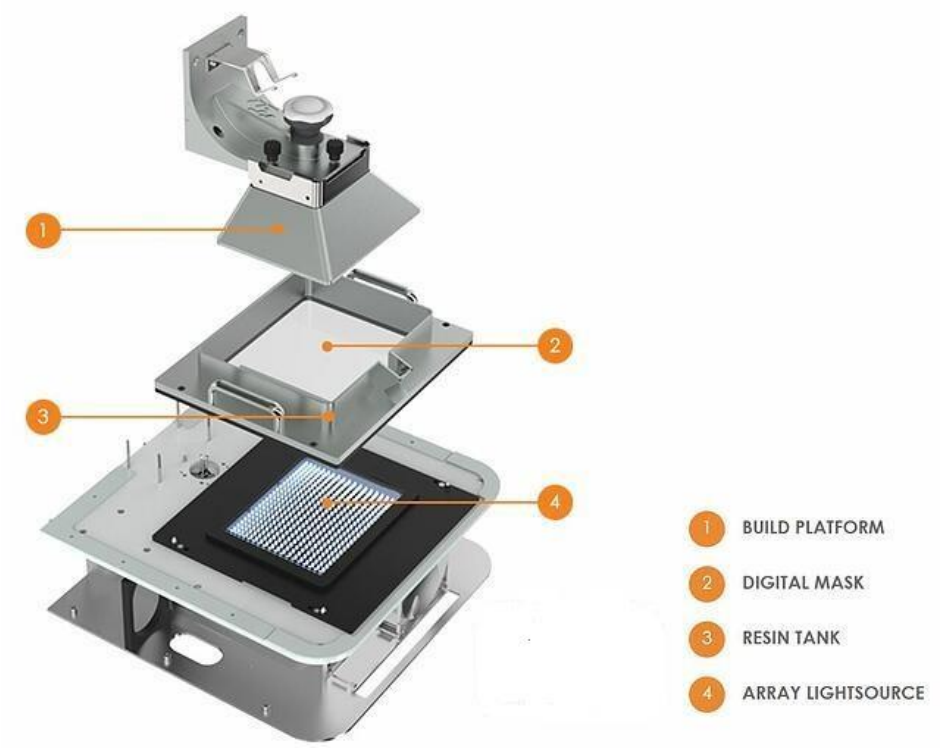

Figure 4.5: MSLA technology components

In this MSLA technology, resin liquid-based materials are used for printing. The resin materials come in various colors (pink, green, black, gray).One of the advantages of using resin is it doesn't need heat for printing like FDM printing, where printing is done by melting the plastic at high temperatures(180 to 270 degrees). The standard gray UV Photopolymer Resin is used for the experiment.

Table 4.3: Some general features of the UV photopolymer Resin

Brand Name	ELEGOO
Color	Grey
Volume	500g
Material	Resin

Hardness	84 D; Shrinkage: 7.1 %
Viscosity (25°C)	150-200 mPa.s
Liquid Density	1.100 g/cm^3
Solid Density	1.195 g/cm^3
Flexure Strength	59-70 Mpa
Extension Strength	36-53 Mpa
Elongation at Break	14.2
Shelf Life	1 year

Furthermore, the resolution is high in resin printing which is the result matrix light source consisting of 28 (50Watt) UV LED lights that have uniform light emission. It has a 25% less layer exposure time and superior result in quality for this technology. Mars Pro is one of the first resin 3D printer that uses the .ctb format for slicing files, which reduces the file size by an average of 90% compared to the .cbddlp format and for this the printing success rate increased in the case of large models.

4.2 Software tools using in the process

Different software tools are needed for drawing analyzing and comparing the experimental data. From drawing CAD tools to getting and analyzing data like Insight 4G with micro-PIV or NOVA 2.1 for FRA analysis needed for different stages of the experiment.

4.2.1 Solidworks 2019

The Solidworks CAD software is a mechanical design automation application that is used for the 3D printing drawing in the experiment. It allows designers to quickly sketch out ideas, experiment with features and dimensions, and produce models and detailed drawings.

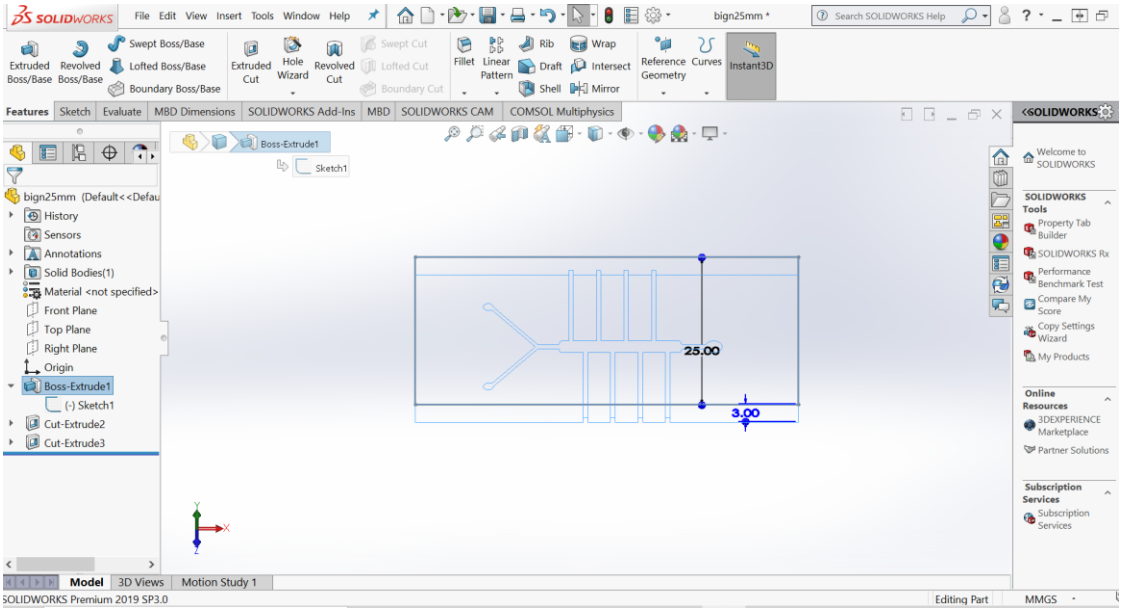

Figure 4.6: General features of solid work 2019

The drawing was created in the front plane and on the ZX axis. In the sketch the 2D design is drawn using its different features and then create 3D part and assemblies' part by part. The design process usually involves the following steps:

- Identify the model requirements.
- Conceptualize the model based on the identified needs.
- Develop the model based on the concepts.
- Analyze the model.
- Prototype the model.
- Construct the model.
- Edit the model, if needed

4.2.2 CHITUBOX Basic

CHITUBOX 64 basic version is a full featured 3D printing preparation tool which is designed to edit and slice that get from solidworks..

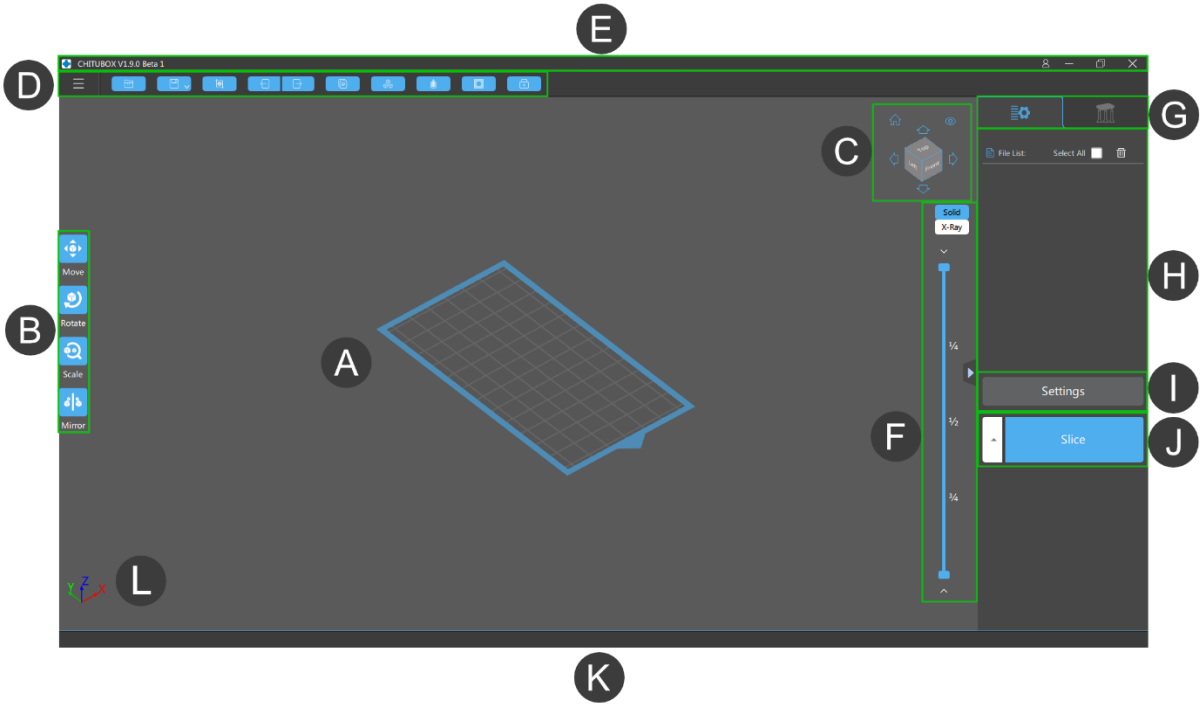

Figure 4.7: Different parts in the chitu box 64

This tool has many features like editing, rotation, scaling, mirroring, repairing, hole digging, cloning etc. to help to get the perfect result. In figure 4.7, different parts of the software are shown.

A. Viewport
B. Left-Side Tool Bar
C. Viewport Cube
D. Menu Panel
E. Title Bar

F. Sliced Preview Slider

G. Switch File List or Support Setting

H. File List or Support Setting

I. Setting

J. Slicing Profile Panel

K. Bottom Status Bar

L. Global Axis

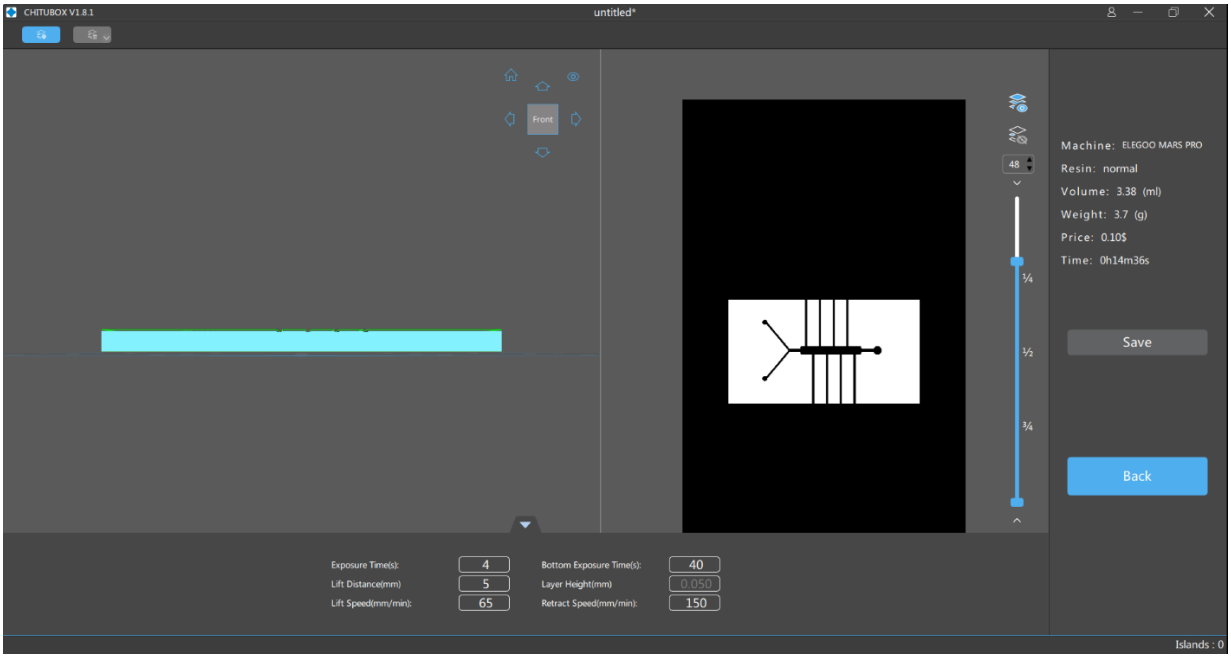

Figure 4.8: Slicing features in the CHITUBOx 1.8.1

The drawing was imported in .stl file from solid work to chitubox for slicing. The exposer time, lifting speed and distance, resin features all theses can modify in the settings. In figure 4.7 it can be seen that the exposure time for our model is 4sec and lift speed is 65/min and the bottom exposer time is 40 sec. In the slicing part, also shows time, volume, weight, and price estimation which can be seen on the right side of figure 4.7.

4.2.3 COMSOL Multiphysics

COMSOL Multiphysics is a simulation tool that has a vast application in the engineering and science field. A model can be created for use in specialized application areas or engineering fields. In the microfluidic are, a it is known for creating various design and analyzing different flow interfaces. Mainly velocity field and electric field were solved by using the Finite Element Method (FEM). Flow is considered Newtonian, incompressible, laminar and steady flow. To see the flow direction a V electrode is designed and simulated in the COMSOL .

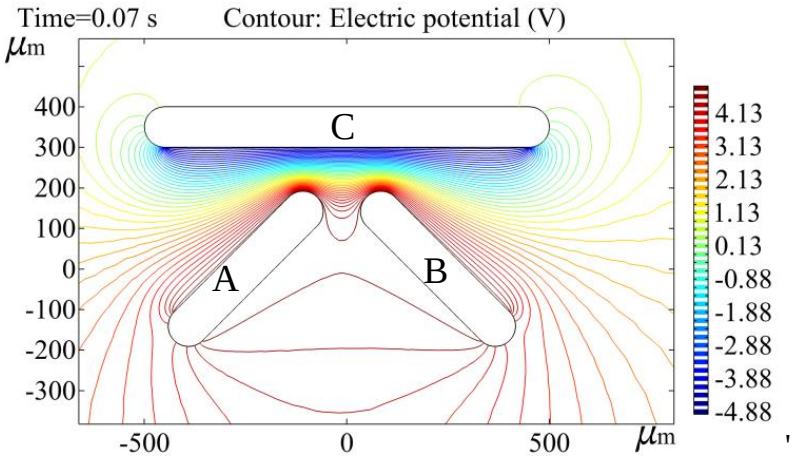

Figure 4.9: Electric Field Distribution Between the electrodes.

The electric field line distribution between the V-electrodes (A&B) and the horizontal electrode (C) is shown in figure:4.1 shows. To analyze the electric field a potential of 5V was applied to the electrodes. The distance between the two V-shaped electrodes was about 50µm for simulation purposes and the between the V-electrodes and horizontal electrode it was 100µm.

As the electric field changes its direction and range fluid particle will also move in this area if applied. If fluids are applied without potential differenences, they will flow

simultaneously and even maybe not flow at all in the case of micro or nano fluids. After applying potential, the perturbation can be seen in the fluids.

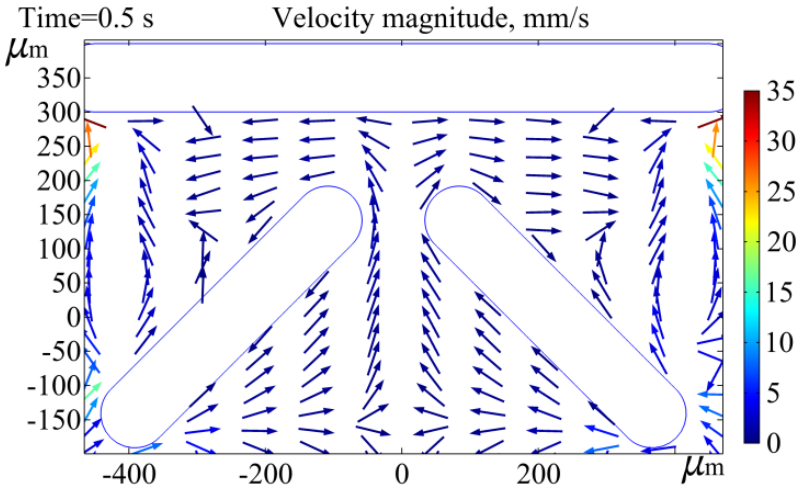

Figure 4. 10: Direction of Fluid Particles After Applying Electric Field

4.2.4 NOVA 2.1

NOVA 2.1 software is an electrochemistry software released by Metrohm Autolab, which is installed and used to control Autolab potentiostat/galvanostat data. This software provides a large range of data handling and analysis tools that can be used to process measured data and apply analysis methods. The frequency response analyzer (FRA) measurement control panel let us simulate and measure the frequency response of the given range for our models.

In the experiment the initial frequency was 0.1 Hz which interprets the frequency for the first AC signal that applied during data acquisition. The final frequency defines the frequency for the last AC signal applied during data acquisition which was 1 MHz here and is the highest range of this component.

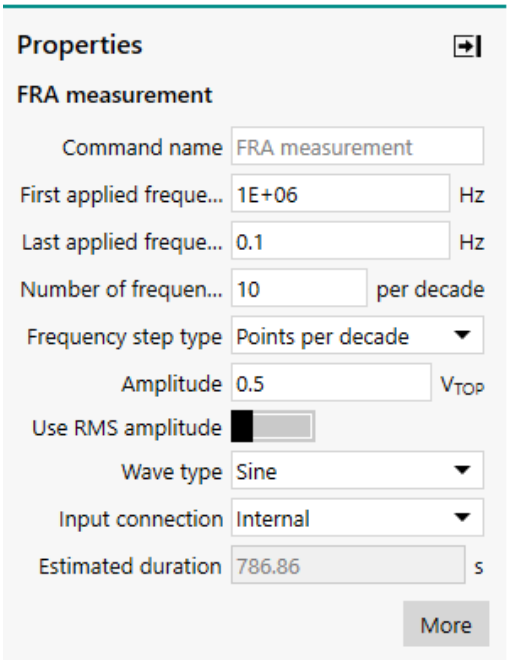

Figure 4.11: Setting parameter in NOVA 2.1

The amplitude was set at 0.5 $V_{Top,}$ and wave type was chosen as sine. When these settings were decided, it must be taken into account the estimated time as it showed at the bottom.

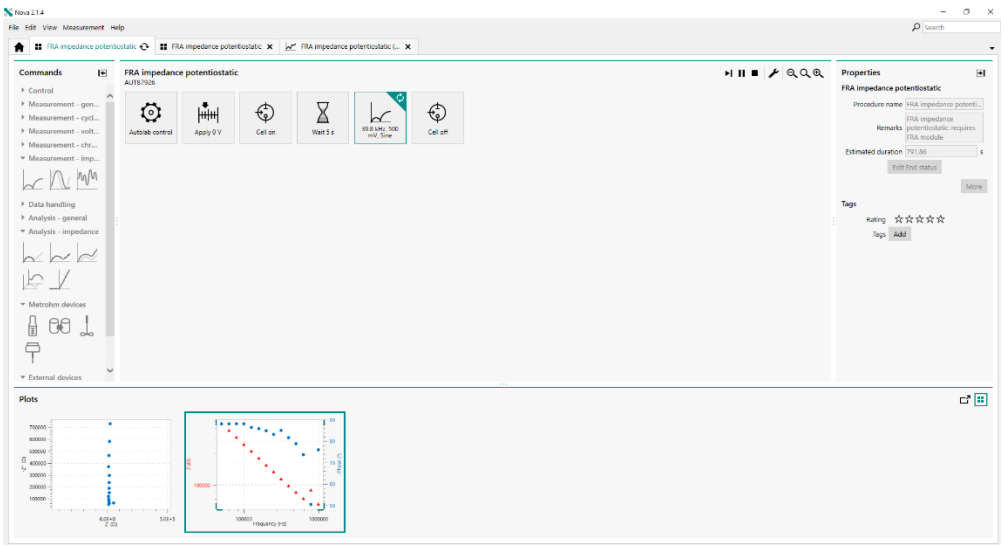

Figure 4.12: FRA analysis in the NOVA 2.1

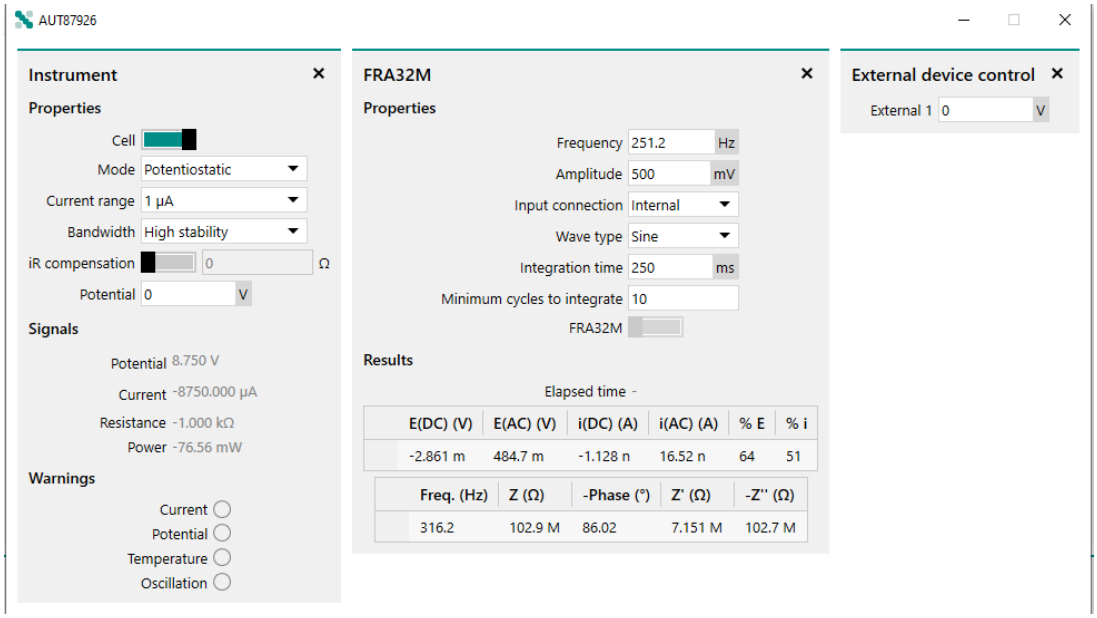

Figure 4.13: Observation of the process in the running EIS process

In the running process several parameters were observed to understand the ongoing process and how it continues. In it, the results can be seen continuously and can get an estimate of the AC/DC values, frequency range, impedance, phase in the process.

Two sets of data were found in this analysis which represent two different wave form. One is the Bode plot and another is the Nyquist plot. Besides this one complete set of data is also shown in numerical form which can be exported for further analysis.

4.2.5 Insight 4G/ Techplot

Insight 4G is a software of imaging, acquisition, analysis and display the results got from micro-PIV which is used for fluid mechanics research in particle sizing measurement. It is used for PIV measurements and is functionally divided into two parts- an acquisition and processing part and a presentation part.

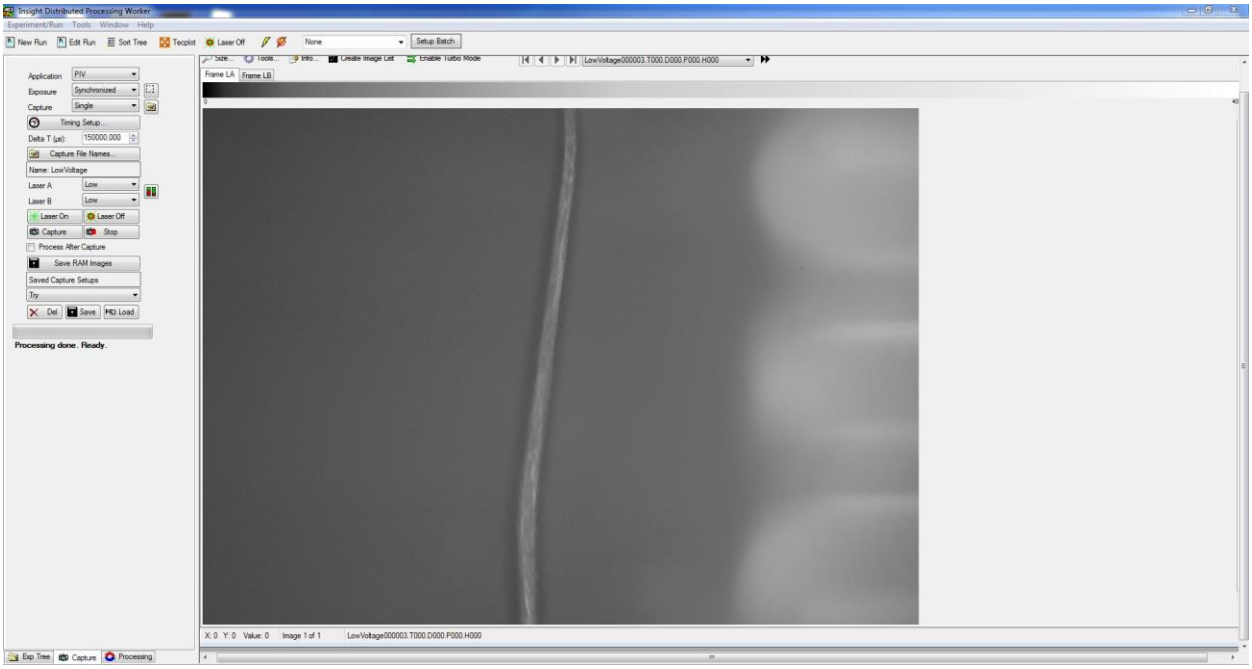

Figure 4.14: data acquisition from the Insight 4G

The first section of this software acquires an image and processes it to obtain different properties such as temperatures, velocity vectors, or concentration information. The second part, displays these results which can be enhanced for optimal viewing. It takes a picture of a sequence and helps to analyze the velocity and direction of the particles.

The desired flow field is illuminated by a powerful laser source (light wavelength, 532 nm). The tracer (fluorescent microbeads) particles are excited by the incident laser light. Additional tools such as Tecplot are used for viewing additional information of the flow field.

CHAPTER V

DEVICE FABRICATION AND FAMILIARIZATION

In this section all the device fabrication process is described in a different section.

5.1 Orthogonal Electrode pattern

To assemble this orthogonal microelectrode device a pair of electrodes is needed which should be aligned perpendicular to each other in the front plane of a glass slide to form a "T" shape. Here, the diameter of the electrode is 0.203mm and they are separated by around 0.6m. For the electrolyte fluids, a perfusion chamber is implemented on the top of the electrodes with 8×9 diameters and a depth of 0.6mm

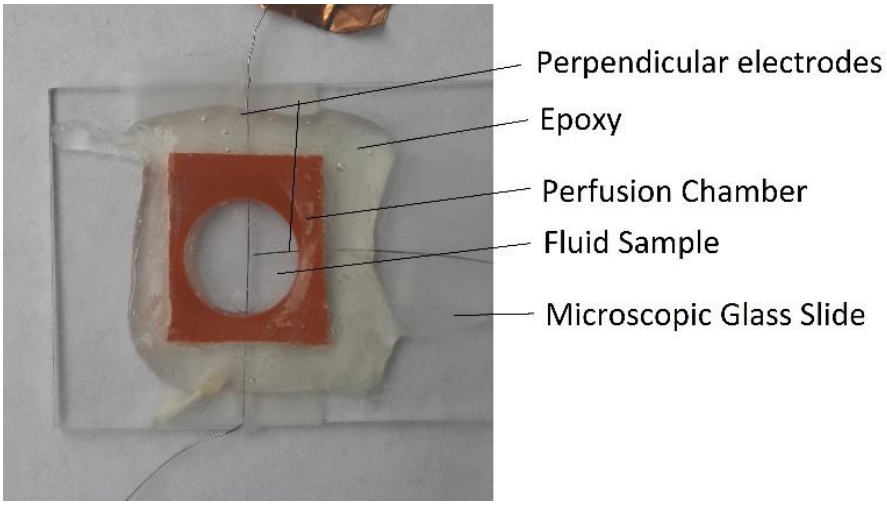

Figure 5.1: Electrode arrangement in the glass slide of orthogonal or "T" sha

5.2 V-shaped electrode Pattern

In this case, the fabrication process has similarities with the previous one. The horizontal electrode was fixed as before and two sharp tip electrodes with a tip radius of 0.5µm and shank diameter of 0.508mm are set at an angle of approximately 45º to the horizontal one. All the other arrangements like perfusion chamber, epoxy is set up like before and copper tape is used to join both sharp tip electrodes to give connection.

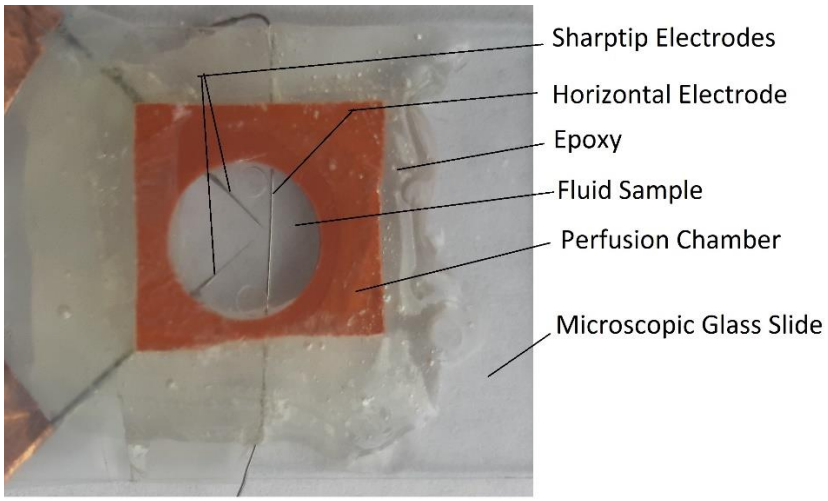

Figure 5.2: electrode arrangement in the glass slide of "V" shaped

5.3 Array Electrode pattern

When we try to organize several electrodes to get the desired arrangement it is not feasible to organize them manually. That is why 3D printing is used to create the expected model of microchannel where we could put the electrodes simultaneously.

Solidworks CAD tool is used for the 3D design. The array electrode pattern has total of 8 electrodes, 4 electrodes on each of the sides. It is designed as a zig-zag in the interface from one to another.

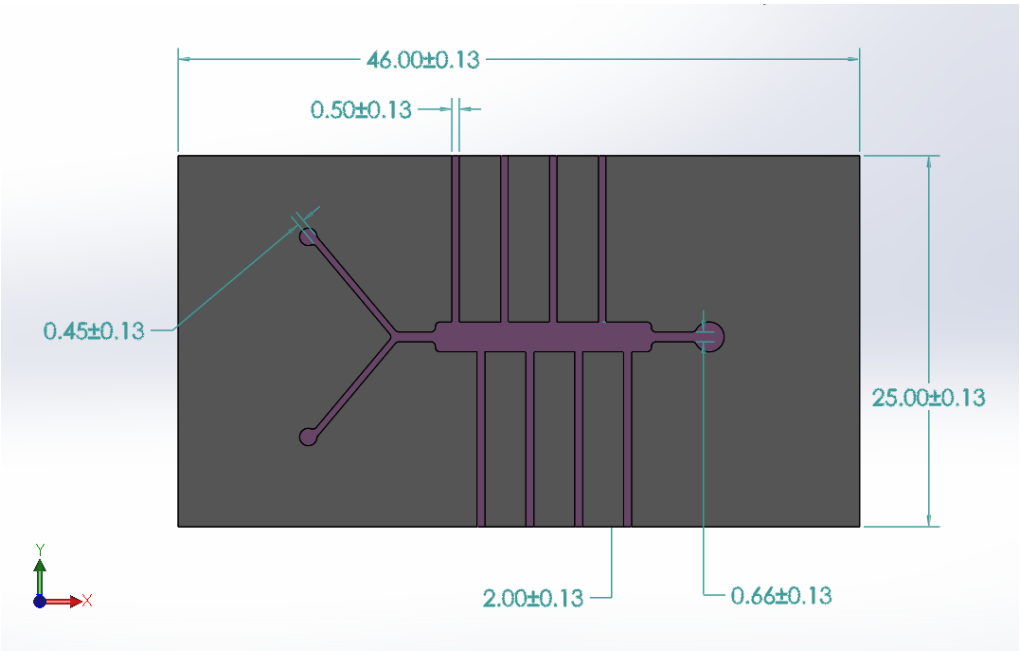

Figure 5.3: Design of the Array electrode with the dimension shown in the Solidworks

The design was created in a base platform that was 25mm wide and 46mm long with a depth of 3mm. The width is designed to insert and sit the sharp tip electrode perfectly.

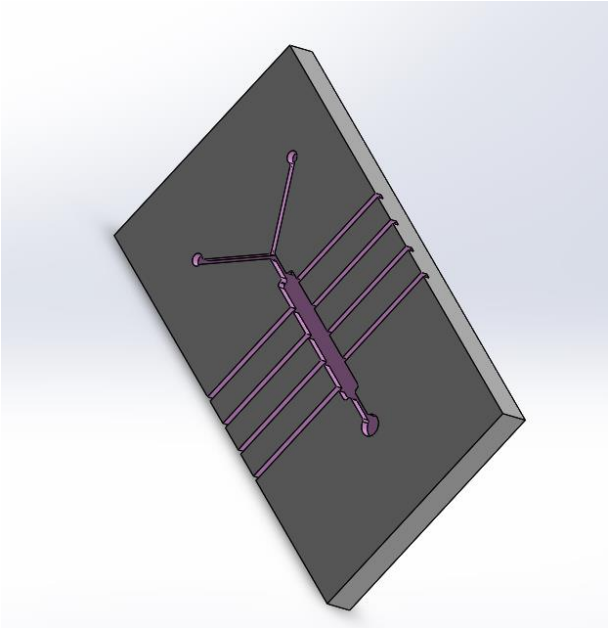

Figure 5.4: 3D view of the microfluidic channel

There is a grooved arrangement for inserting the electrodes in Array shaped which is 2mm apart from each other There are two inlets and one outlet was designed so that the microchannel can be used in different forms. The normal width was 0.66 mm in the micro channel which get bigger in the electrode space upto 2mm width. While the depth of the cut for the whole microchannel is 0.75mm the cut for the electrode is 0.5mm to set the electrode properly. The diameter of the inlets and the outlets are 1.5mm and 2mm respectively. After getting the decided design and slicing it in the CHITUBOX the Design is transferred to a 3D printer to get the device.

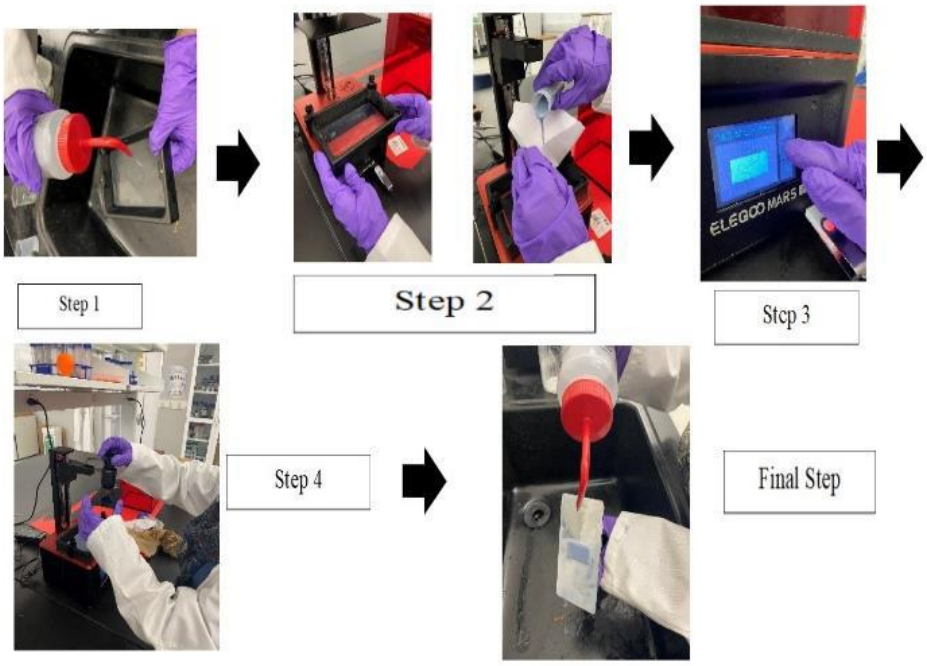

Figure 5.5: Steps of the 3D printing

In the printing process the printer needs to be cleaned. After inserting the design and ideal level of resin in the resin tank the cover should be put. The atmosphere should be darkened as the light can be affected the model. When the printing is started it shows the time duration and the completed layer that was printed.

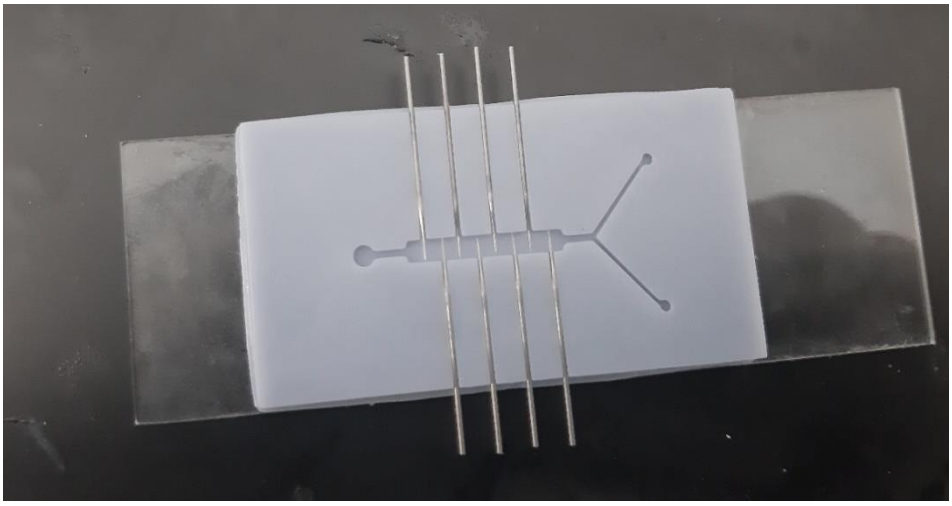

Figure 5.6: Inserted electrode arrangement in an Array pattern in 3D printed microfluidic channel

After finishing the printing, it needed to be washed in acetone to clear and have to dry for further use. After all these processes we can stick the electrode in the channel and get the device to work which is shown in figure 5.6.

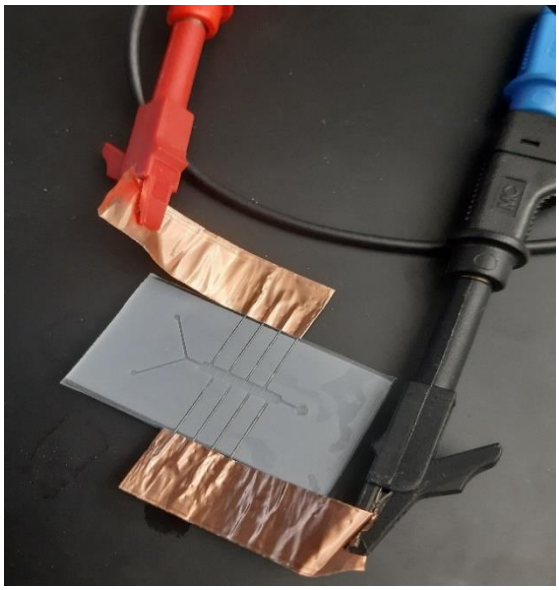

Figure 5.7: Final output of the Array electrode pattern used in the experiments

The electrode needs to be glued with the channel, or it will come out at the time of the experiment. We can use PDMS or glass slides to cover the channel. At last, copper, the tape was used to connect the electrodes with one another and with the source.

5.4 Electrolyte fluids

For the experiment purpose, three different fluids are used with different conductivity ranges. Firstly, De-ionized or DI water has 18.72µS/cm conductivity. The second one is tap water which has a conductivity of 666.12 µS/cm. Lastly, Phosphate Buffered Saline (PBS) was PBS (10×) and later diluted PBS (1×) by adding 45ml DI water with 5ml PBS(10×) solution. The conductivity of PBS (1×) is 8235.24 µS/cm.

CHAPTER VI

RESULTS & DISCUSSIONS

In the results and discussion the obtaining results for each electrode are showan and describe in a continuous pattern. They are all compared with one another for the different application fields. At last the results from micro-PIV are exhibited with the decided explanation for particle manipulation.

6.1 Obtaining Results from EIS

All EIS experiments were carried out using AUTO LAB PGSTATAT302N with the help of the FRA32M module, which is used to create EIS spectra. NOVA 2.1 was used to analyze the values for the measurement of the experiment. All the values that took in the FRA measurement of NOVA 2.1 were in the fixed range to observe the behavior of the electrodes and fluids. We have done our work and comparisons for EIS in different stages. In the 1st stage, we got data from T or orthogonal electrode patterns for three different fluids with diverse conductivity ranges and compared their results and pattern. These three experimental fluids DI water, tap water, and PBS 1x solution, have three different conductivity ranges: 18.72 µS/cm, 666.12 µS/cm and 8235.24 µS/cm, respectively. In the next stage we did the same experiments for V-shaped electrodes and compare their results both among themselves and also with the previous results we got for T electrodes.

6.1.1 For T or Orthogonal Electrode Pattern

For T or orthogonal electrode pattern we run the EIS analysis for all three electrodes. For get an accurate result, we run each analysis several times. As EIS analysis is really sensitive sometime ist shows some ripple effect. For each analysis we get a set of data where total impedance(Z), phase(Φ), Time (T), the real part of the impedance(Z') and imaginary part of the impedance(Z'') are given in a bundle for each set of frequencies and these frequencies are same for the same range of it. The data set can be exported as an excel file to compare and analyze.

Table6.1: EIS data for T or orthogonal electrode pattern and DI water

Index	Frequency (Hz)	Z' (Ω)	-Z'' (Ω)	Z (Ω)	-Phase (°)	Time (s)
1	1000000	60236.26	74672.28	95939.34	51.10775	7.388139
2	794330	90467.23	9116.21	90925.39	5.754162	8.868164
3	630960	61802.54	63707.94	88759.54	45.86975	10.41319
4	501190	72652.31	77638.6	106330.2	46.90024	11.84322
5	398110	88755.84	86421.69	123880.2	44.23661	13.30824
6	316230	108802.9	94100.23	143850.4	40.85549	14.90828
7	251190	128309.2	82754.53	152681.3	32.82046	16.3983
8	199530	144991.5	79011.02	165122	28.58754	17.66833
9	158490	159473.7	71281.29	174679.4	24.0836	19.00836
10	125890	170235.7	62055.23	181193.4	20.02808	20.36838
11	100000	175011.7	57607.38	184249.1	18.21963	21.8084
12	79433	181495.3	49249.32	188058.6	15.18181	23.12343
13	63096	186424.1	42088.13	191116.1	12.72212	24.43845
14	50119	189972.4	36152.05	193381.7	10.77465	25.85848
15	39811	192823.9	31347.02	195355.3	9.233688	27.2335
16	31623	194922.6	27551.77	196860.1	8.045304	28.62853
17	25119	196646.9	24762.62	198199.9	7.177154	30.01356
18	19953	197654.9	22542.15	198936.2	6.506359	31.35858
19	15849	199000.1	21611.35	200170.2	6.198013	32.74861
20	12589	200349.1	21413.25	201490.2	6.100596	34.04863
21	10000	201702.4	21944.93	202892.7	6.209276	35.35365
22	7943.3	203025.5	23195.07	204346.1	6.517617	36.67368
23	6309.6	204731.3	25158.61	206271.3	7.005727	38.0287
24	5011.9	206516.8	27886.97	208391.1	7.69041	39.31873
25	3981.1	208584.4	31428.15	210938.9	8.568502	40.68875
26	3162.3	211089	35835.22	214109.2	9.634877	42.07878

27	2511.9	214215.1	41209.6	218142.9	10.88924	43.4738
28	1995.3	217665	47561.91	222800.8	12.32594	44.81883
29	1584.9	221898.5	55072.19	228630.5	13.9384	46.17385
30	1258.9	226919.7	63872.99	235737.8	15.72076	47.57888
31	1000	232660.4	74043.05	244158.2	17.65342	48.93391
32	794.33	239665.2	85884.61	254589	19.71526	50.20393
33	630.96	247610.2	99444.17	266833.2	21.88117	51.51895
34	501.19	257015.1	115009.7	281574.1	24.10767	52.88398
35	398.11	268250	132849.9	299344.6	26.34676	54.254
36	316.23	281334.8	153050.8	320271.5	28.54693	55.51903
37	251.19	296875.7	175984.4	345116.9	30.65896	56.87405
38	199.53	315003.8	201828.2	374115	32.64837	58.21908
39	158.49	335793.2	230714.7	407414.2	34.49194	59.5991
40	125.89	358487.3	261944.5	443991.1	36.15537	62.02915
41	100	386288.1	298950.3	488456.5	37.73647	63.32917
42	79.433	418671.1	340878.8	539892.4	39.15221	64.7042
43	63.096	453461.2	388669.9	597236.4	40.60048	66.21922
44	50.119	494573.4	439505	661640.1	41.62604	67.73425
45	39.811	541169	501455.3	737781.4	42.81865	76.72942
46	31.623	595918	571753.8	825845.4	43.81447	78.41945
47	25.119	661663.6	654917.3	930975.5	44.70641	80.16448
48	19.953	733239.6	747171.1	1046855	45.53917	82.17452
49	15.849	815389.1	853036.6	1180055	46.29264	84.34956
50	12.589	909418.1	975031.8	1333315	46.99415	86.7346
51	10	1015742	1114902	1508224	47.66464	89.44465
52	7.9433	1137120	1277281	1710114	48.3224	92.58971
53	6.3096	1276934	1466626	1944622	48.95517	96.25478
54	5.0119	1435924	1686846	2215248	49.59398	100.6249
55	3.9811	1617919	1943438	2528757	50.22251	105.81
56	3.1623	1826551	2243359	2892913	50.84739	112.1601
57	2.5119	2066356	2595470	3317573	51.47532	119.8652
58	1.9953	2343109	3010116	3814572	52.1024	129.1854
59	1.5849	2649007	3488963	4380651	52.7923	146.4557
60	1.2589	3009278	4052868	5047919	53.4059	160.471
61	1	3426676	4717078	5830346	54.00383	178.2463
62	0.79433	3917050	5498455	6751022	54.53427	197.3667
63	0.63096	4489953	6413700	7829127	55.0058	218.632
64	0.50119	5182386	7518608	9131626	55.42249	242.4175
65	0.39811	5970060	8778368	10616090	55.78086	269.583
66	0.31623	6902725	10260306	12366143	56.06891	300.7936
67	0.25119	8013484	12010717	14438603	56.289	337.4242
68	0.19953	9338155	14071109	16887784	56.43015	380.575
69	0.15849	10912045	16472745	19759151	56.4783	431.926
70	0.12589	12800046	19292184	23152312	56.43638	493.7621
71	0.1	15048245	22535836	27098221	56.26709	568.6435

As given here for each analysis we get a similar table where these seventy-one frequencies are common and for each frequency, we get different data for their electrode and liquids.

When taking the values of each step NOVA 2.1 also generates both the Nyquist plot and Bode plot simultaneously. These originated graphs can also export as PNG files.

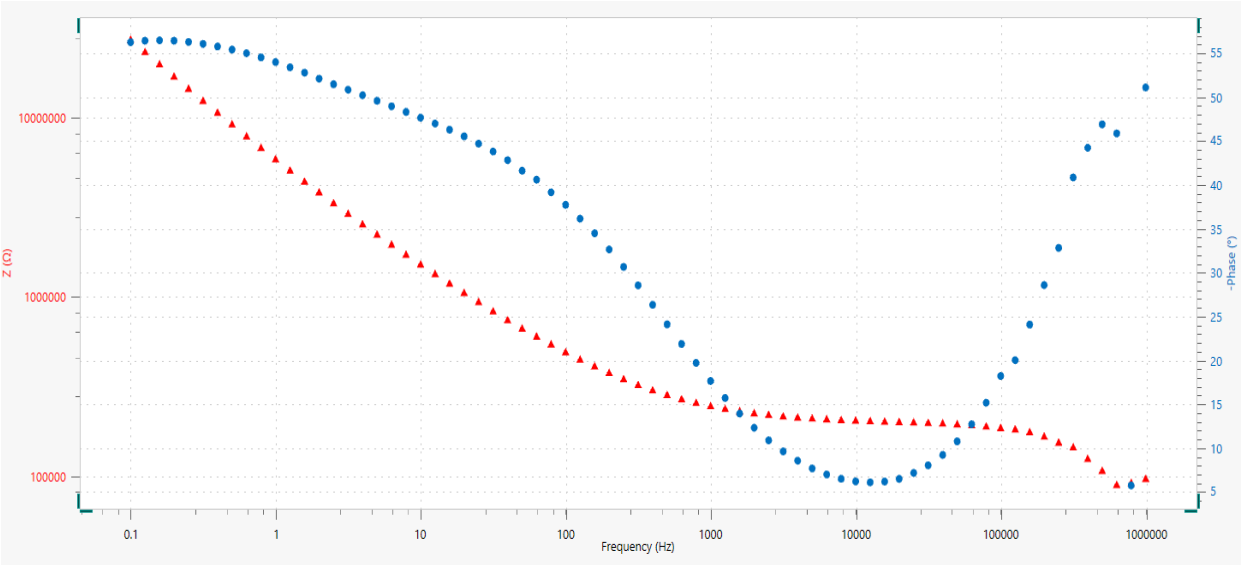

Figure 6.1: Bode plot generated from NOVA 2.1for T electrode and DI water

In the Bode plot both the impedance and phase shift is plotted in the same graph against the frequency range from 0.1Hz to 1MHz. Here impedance is shown in red color and phase shift as blue color, and for each frequency, in the FRA measurement one dot is plotted and thus make this graph. One of the main advantages of this plot is that we can see the result visually of how each frequency crates each dot of the phase shift and impedance, which is difficult to determine in the Nyquist plot. In the Bode plot, a phase angle of -90º and impedance slope -1 refer a pure capacitance, but in the real case, both capacitive and resistive characteristics are present in the

case of electrochemical and that is why the value of the phase angle fluctuates from 0º to -90º [Zhan H. et al.].

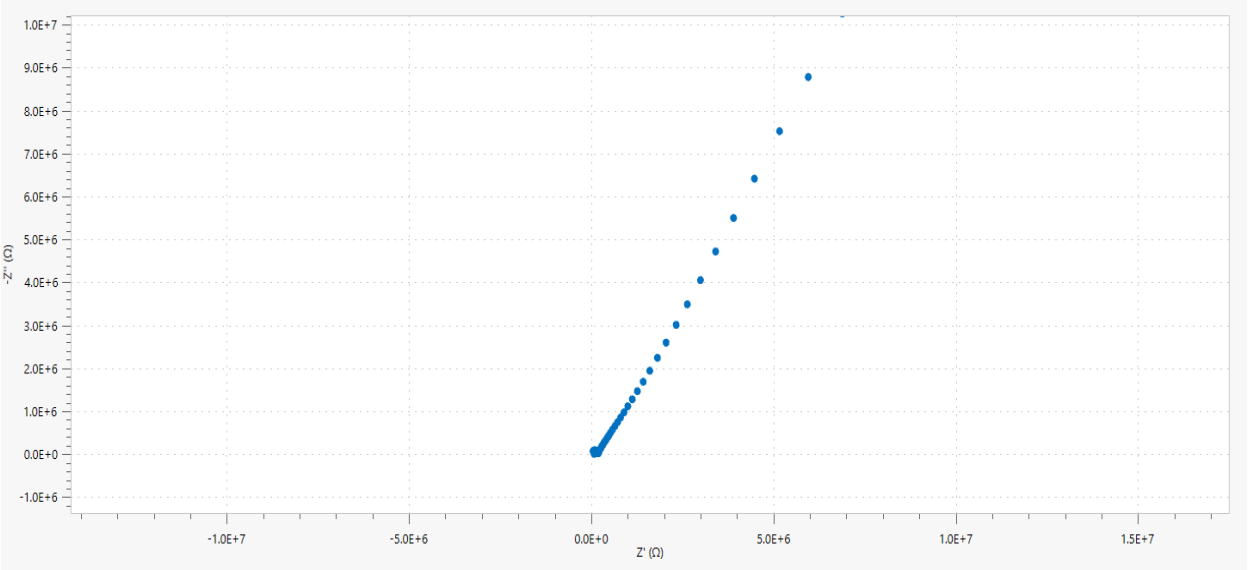

Figure 6.2: Nyquist plot generates in Nova 2.1 for T electrode and DI water

The complex value of impedance is transcribed in terms of the real and imaginary values in a certain range of frequencies. In this case, the T electrode creates a half-circle than a huge linear part after that up to 1×10^{7}in the imaginary part in the y-axis. On the other hand for the real part it goes up to 6×10^{6} in the x-axis. For its large range its hard to see the semicircle in the high range of frequency. In absence of the redox probe, the real part of the impedance(Z') indicate the ionic molecular concentration for the electrode material and the imaginary part of the impedance(Z'') refers to the capacitive quality of the bulk medium [Zia A.I et al.].

Like DI water we also get each set of seventy-one data for Tap water and PBS 1x solution for further analysis. At the same time we also export the plots of all three solutions for comparison and analysis purposes.

6.1.2 For V -Shaped Electrode Pattern

For the V shape electrode we run the EIS analysis like before and get each set of data for DI water, Tap water, and PBS 1x solution. Like previously we showed one set of data for DI water in the case of V-shaped electrode and as it can be seen every time the values change for different electrodes and different fluids. For the V electrode, the frequency stops are same but both the starting value of the impedance(Z) and the phase(Φ) are quite lower than before.

Table 6.2: EIS data for V-shaped electrode pattern and DI water

Index	Frequency (Hz)	Z' (Ω)	-Z'' (Ω)	Z (Ω)	-Phase (°)	Time (s)
1	1000000	14228.63	6444.781	15620.15	24.3679	7.091133
2	794330	14887.3	3941.928	15400.34	14.8307	8.541157
3	630960	15055.59	5094.388	15894.13	18.69438	10.09119
4	501190	15835.35	4520.378	16467.92	15.93199	11.51121
5	398110	16350.54	3825.842	16792.17	13.16963	12.96124
6	316230	16676.48	3166.62	16974.46	10.75163	14.55627
7	251190	16742.96	2521.522	16931.77	8.564493	16.06129
8	199530	16836.66	2074.289	16963.95	7.023492	17.30132
9	158490	16835.57	1688.938	16920.07	5.728725	18.62634
10	125890	16762.33	1382.209	16819.22	4.713899	19.98137
11	100000	16507.61	1601.687	16585.13	5.541903	21.41139
12	79433	16447.05	1340.789	16501.61	4.660536	22.71142
13	63096	16367.98	1149.361	16408.28	4.016722	24.01644
14	50119	16248.15	1012.916	16279.69	3.567226	25.43647
15	39811	16148.5	926.4522	16175.06	3.283504	26.75649
16	31623	16040.02	881.6984	16064.23	3.146306	28.13152
17	25119	15929	873.4282	15952.93	3.138533	29.51155
18	19953	15842.61	899.8385	15868.15	3.250828	30.81657
19	15849	15767.43	957.117	15796.46	3.473714	32.12159
20	12589	15710.24	1044.267	15744.91	3.802882	33.39662
21	10000	15652.52	1164.625	15695.79	4.255247	34.72664
22	7943.3	15620.73	1308.568	15675.44	4.788558	36.02666
23	6309.6	15619.58	1479.981	15689.54	5.412709	37.32669
24	5011.9	15647.26	1678.997	15737.08	6.124574	38.64172
25	3981.1	15726.02	1905.633	15841.06	6.909248	39.92674
26	3162.3	15829.13	2160.139	15975.84	7.770927	41.30676
27	2511.9	15963.69	2438.481	16148.86	8.684892	42.69179
28	1995.3	16146.73	2738.291	16377.27	9.6251	43.97681

29	1584.9	16368.25	3058.928	16651.62	10.58544	45.28684
30	1258.9	16632.98	3396.061	16976.14	11.53983	46.61186
31	1000	16949.18	3747.607	17358.55	12.46798	47.87689
32	794.33	17321.64	4117.039	17804.19	13.37008	49.13691
33	630.96	17747.58	4501.69	18309.61	14.23295	50.39193
34	501.19	18196.78	4903.155	18845.79	15.08029	51.76196
35	398.11	18711.35	5333.153	19456.54	15.90874	53.08698
36	316.23	19248.23	5785.978	20099.05	16.73067	54.31701
37	251.19	19826.4	6278.864	20796.88	17.57258	55.66203
38	199.53	20462.36	6826.184	21570.93	18.44855	56.96205
39	158.49	21133.36	7430.468	22401.58	19.37162	58.22708
40	125.89	21849.32	8111.557	23306.44	20.36743	59.5721
41	100	22648.33	8888.216	24329.96	21.42726	60.92713
42	79.433	23507.8	9787.247	25463.83	22.60393	62.24715
43	63.096	24430.4	10830.76	26723.58	23.9092	63.65218
44	50.119	25184.55	12021.36	27906.54	25.51658	65.1122
45	39.811	26137.71	13467.3	29403.2	27.25951	74.07237
46	31.623	27401.33	15158.98	31314.98	28.95227	75.6324
47	25.119	28737.37	17128.25	33454.65	30.79608	77.40243
48	19.953	30190.52	19442.36	35909.23	32.78108	79.36247
49	15.849	31832.72	22172.62	38793.65	34.85858	81.53751
50	12.589	33522.31	25274.44	41982.65	37.01479	85.28758
51	10	35636.87	29070.05	45989.72	39.20514	87.88762
52	7.9433	38109.47	33549.66	50773.13	41.35907	91.00768
53	6.3096	40991.81	38824.15	56459.21	43.44434	94.66775
54	5.0119	44396.54	45041.16	63243.65	45.41295	99.07283
55	3.9811	48459.58	52359.99	71343.53	47.2155	104.3129
56	3.1623	53401.56	61039.78	81102.29	48.81846	110.528
57	2.5119	59583.8	71481.01	93057.85	50.18673	118.1782
58	1.9953	66931.3	83490.46	107006.8	51.2821	127.4234
59	1.5849	77085.06	98325.14	124939.7	51.90422	138.7836
60	1.2589	88532.76	114962.9	145101.8	52.40019	152.9038
61	1	102412.4	133970.5	168631	52.60426	170.6242
62	0.79433	119145.7	155566.7	195950.8	52.55215	189.7445
63	0.63096	139360.5	179759.5	227452.9	52.21497	210.9549
64	0.50119	163602.1	206647.5	263569.4	51.63147	234.7153
65	0.39811	192474.2	236102.5	304615.6	50.81258	261.8408
66	0.31623	226486.6	267850.6	350770.7	49.78312	293.0014
67	0.25119	266688.9	301986.5	402888.1	48.55178	329.3871
68	0.19953	312957.7	337181.5	460036.8	47.13382	413.1737
69	0.15849	366948.4	375298.7	524881.1	45.64456	464.3496
70	0.12589	429324.7	420351.3	600845.2	44.39493	525.9907
71	0.1	504552.1	477462.2	694653.1	43.41984	600.6371

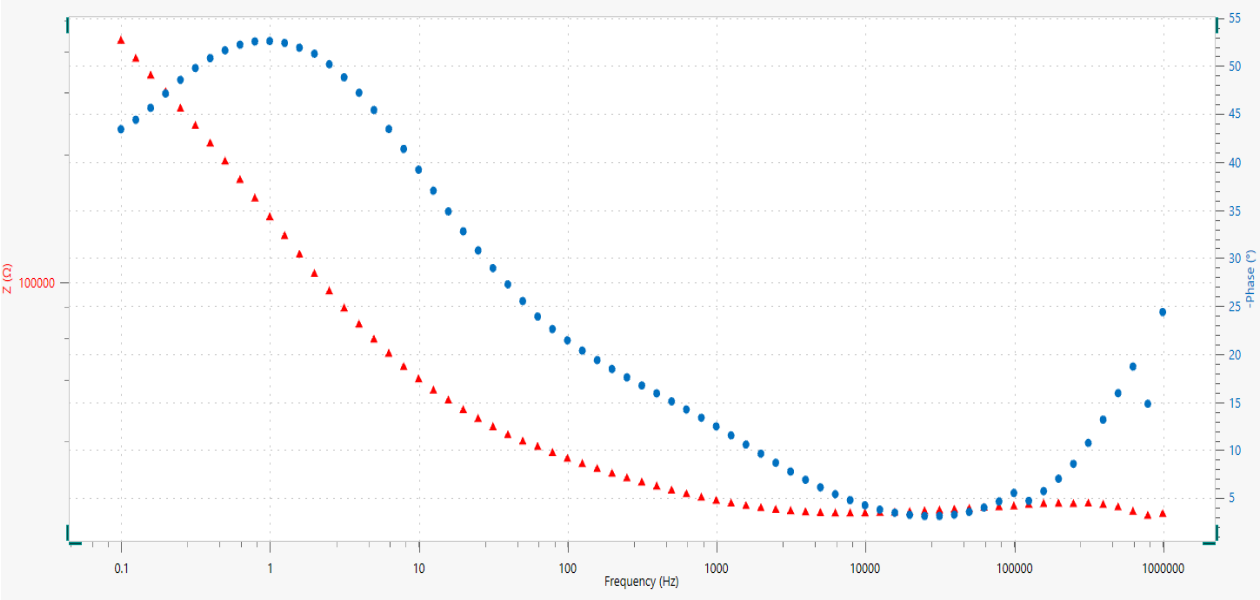

Figure 6.3.: Bode plot generated from NOVA 2.1for V electrode and DI water

As we can see in the bode plot here for V electrode, the pattern is same but the nature, staring point, intersection all these measurements seems different than the previous one.

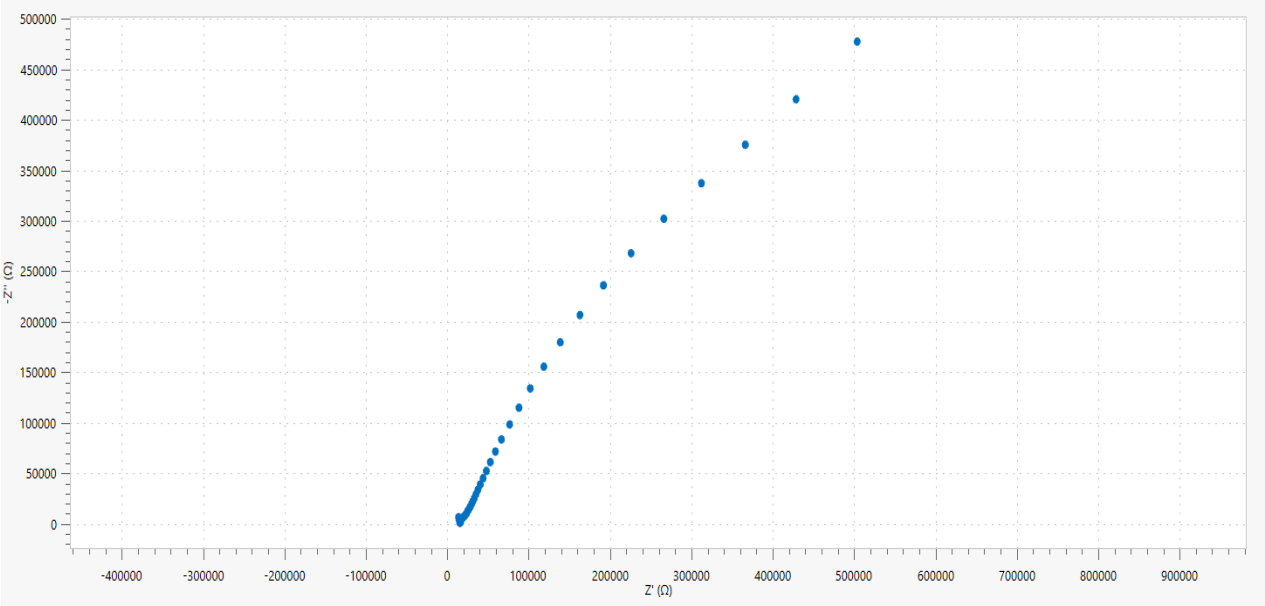

Figure 6.4: Nyquist plot generate in Nova 2.1 for V electrode and DI water

In the case of the Nyquist plot here for V shaped electrode, a large semicircle portion is seeming to crate which is the result of slow electron transfer process. The capacitive value is much larger here than the orthogonal electrode for the same electrolyte. It can be proven beneficial in some microfluidics applications where we need a slow rate of electron transfer for higher detection levels as sensors.

6.1.3 Comparison between T or orthogonal electrode and V -Shaped Electrode Pattern

We can get the bode plot and Nyquist plot from NOVA 2.1 but it is not possible to manipulate or add multiple values in the same graph. That is why we export the values in the excel file to get a comparison graph. To evaluate electrochemical behavior of electrode and electrolyte materials normally two-electrode mode is used in the experiment where potentiostat can be programmed in a large frequency range under EIS function. It is assumed that the properties of the material of the electrodes don't change with time easily and that is why EIS is the basic to determine these properties and their interrelations and their dependences [Barsoukov E et al.].

Previously in Rakesh Guduru et.al and Mohammad Salman Parvez et al. , they illustrate the "T" shaped and "V" shaped electrode and their pattern of flow respectively. We here compare these two patterns in the three experimental fluids to observe the difference because of the kinetics of the electron transfer of the redox probe at the electrode interface.

Both the Bode plot and the Nyquist plot have their strength and lacking. The Bode plot is well known to deliver the results clearly while the Nyquist plot is more complex which doesn't give a clear output of the given frequency in the plots. Still, the Nyquist plot is more popular for

its sensitive behavior in EIS. We evaluate both graphs for comparing the electrode and electrolyte differences.

Comparison in the Bode plot is shown in Figure 6.5 and figure 6.6 and figure 6.7 where all these are mainly the representation of the Bode plots of T and V electrodes in different electrolyte fluidics which simply represents the magnitude and phase.

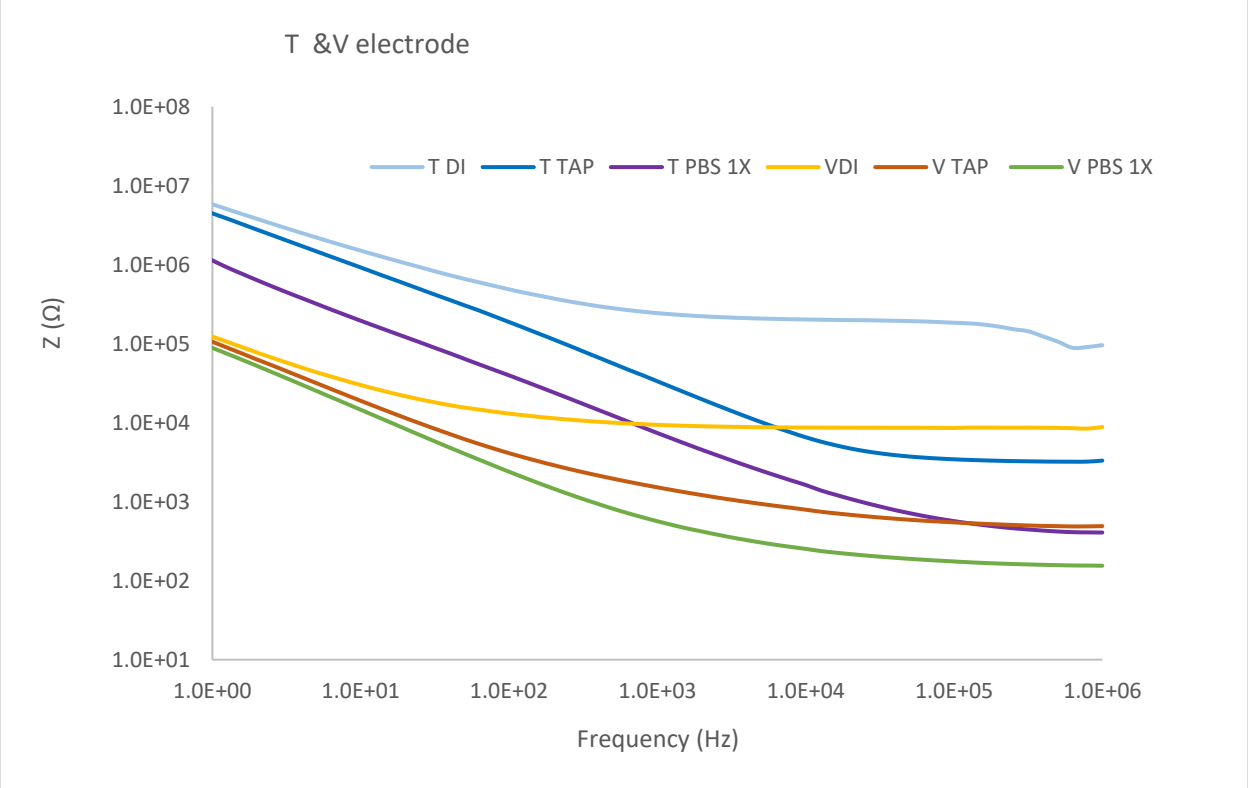

Figure 6.5: Frequency Vs Impedance curve for T and V electrode in three different experimental fluids

The magnitude is the vector quantity $|Z|$ impedance which consists of the real Z_{RE} and imaginary part Z_{IM}. The phase (φ) also consists of these real (Z_{RE}) and imaginary (Z_{IM}) part and the slope of the transformation area in between both asymptotic limits give the idea of the influence of the frequency dependence.

Because of the impedance, the capacitive behavior is generally very high at the lower frequencies. Generally, at lower frequencies, the measurement of impedance mainly depends on the electrolyte solution.

At very high frequencies it depends on mostly the inductance of the electrochemical cell [Katz E et al]. Here, the conventional range (1Hz to 1MHz) is showen and analyzed analytically which is controlled by the interfacial effects of the given electrodes. On the whole, the impedance curve is higher at low frequency (1Hz) and it is getting lower rhythmically with the increase of frequency and has its lowest at the highest frequency(1MHz). It means in all cases the capacitor effect or EDL effect decreases with the increase of the frequency. That also verifies that at the lower frequency we get a high EDL effect (higher zeta potential) and AC electroosmosis dominates.

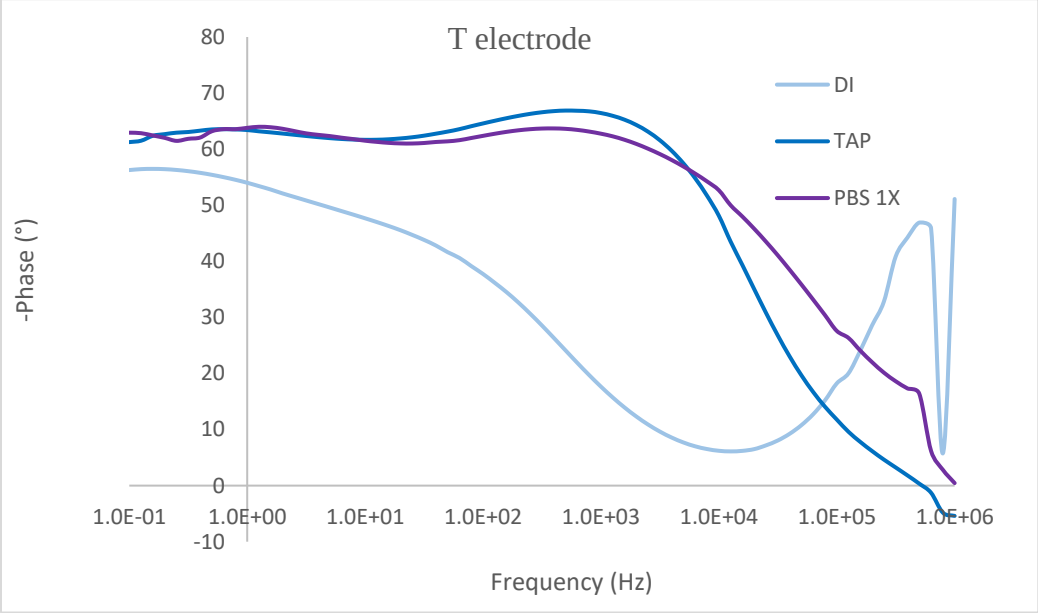

Figure 6.6: Phase shift Vs Frequency curve for three different fluids for the T electrode

In between T and V electrodes for each electrolyte fluids, the impedance is much higher in the T electrode than the V electrode as the capacitive effect sustains longer in the T electrode as EDL. For DI water when the impedance showed 10MΩ in the beginning at 1 Hz, it only reaches 0.1MΩ at that point for the V electrode. It is seen for the other fluids as well. It is because the EDL effect works longer in the T electrode than the V electrode.

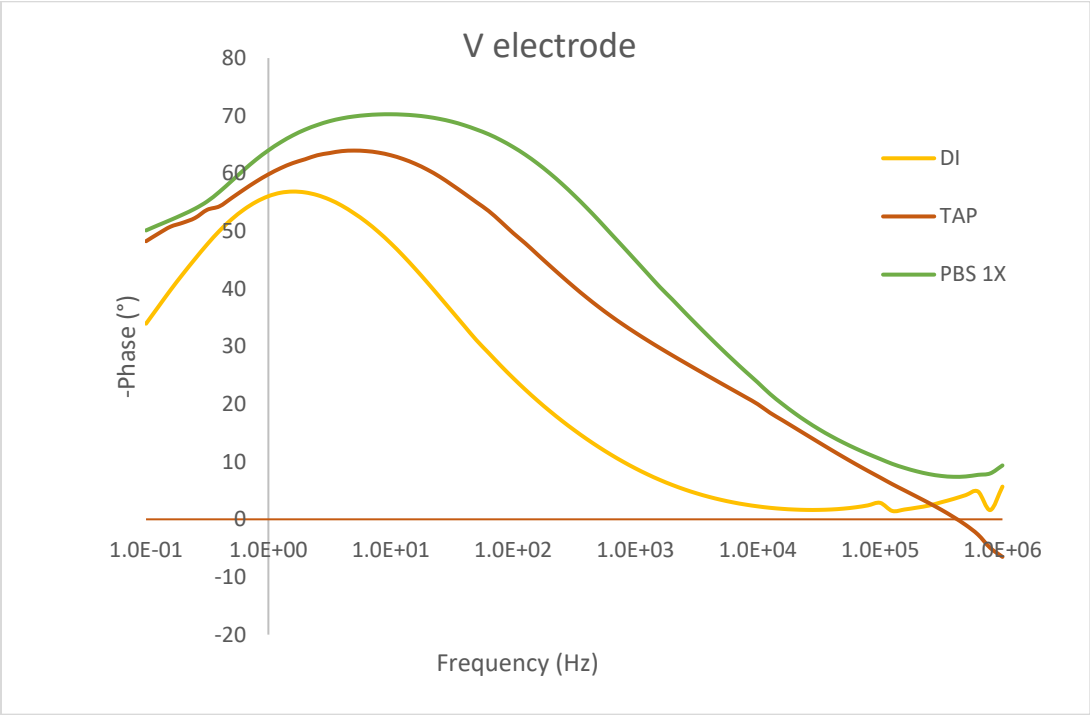

Figure 6.7: Phase shift Vs Frequency curve for three different fluids for the V electrode

In the case of electrolytes, orderly characteristics are exhibited where the conductivity and the impedance have inverse relation between them. As the EDL effect will be lower in the high conductivity it is common to get a lower impedance. The thickness of EDL depends on both the surface charge and ionic strength of the solutions. The highest conductivity electrolyte PBS showed the lowest impedance. At the same time, the lowest conductivity fluid DI water has the highest value in both cases.

In figure 6.6 and 6.7 the phase shift for each value declines with the rise of the frequency. As for pure resistive value, the phase shift should be 0º and for pure capacitive value, this should be 90º. For the V electrode, the phase drops faster than the T electrode which indicates the longer exitance of the capacitive effect in the T electrode.

Figure 6.8 represents the comparison in Nyquist plot. Here, in the T electrode, the output curve of a linear part for this one is due to very fast electron transfer.

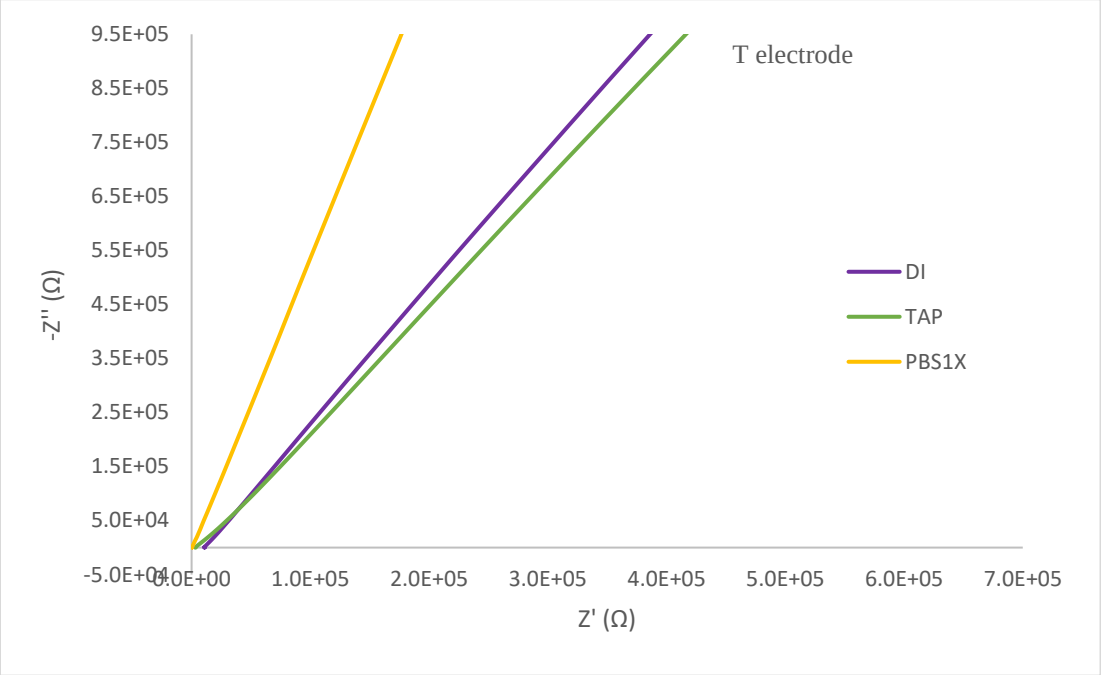

Figure 6.8: Schematic Faradaic impedance spectra which are presented in the form of a Nyquist plot for three different fluids in orthogonal or T electrode

Even though DI water gets a bit more than Tap water value in the graph but PBS 1x exhibits much higher values in the curve for the real part(Z') which indicates its more resistive nature than others. It also verifies us that micro-pumping can be better designed using the "T" electrode pattern compare to the other one.

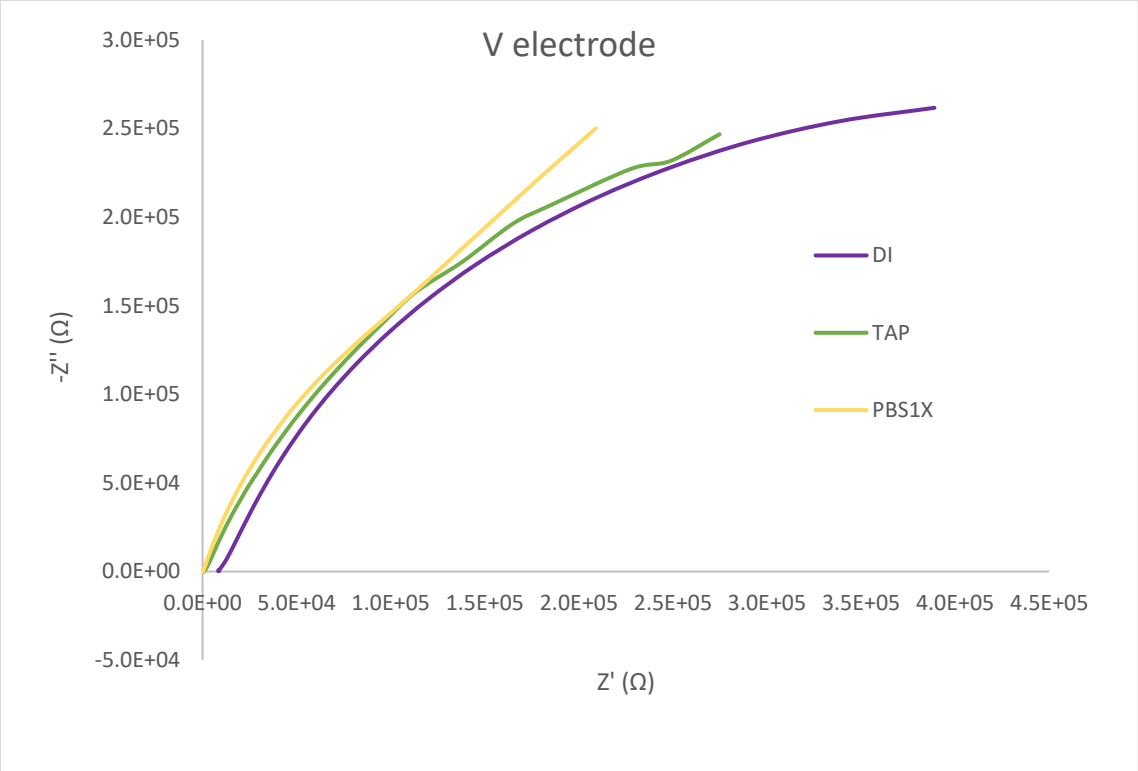

Figure 6.9: Schematic Faradaic impedance spectra which are presented in the form of the Nyquist plot for three different fluids in the V-shaped electrode

In the case of the V electrode, a large semicircle portion is visualized which occurs due to a very slow electron transfer process. It can be proven beneficial in some microfluidics applications where we need a slow rate of electron transfer for higher detection levels as sensors. At first the real and imaginary parts increase with the decrease of frequencies but in the last due to more capacitive characteristics the imaginary part spike up for DI water. In contrast, PBS 1X which contains the highest conductivity, displays more linearity. Here, for smaller electrolyte conductivity the graph manifests a lower frequency range of the dispersion.

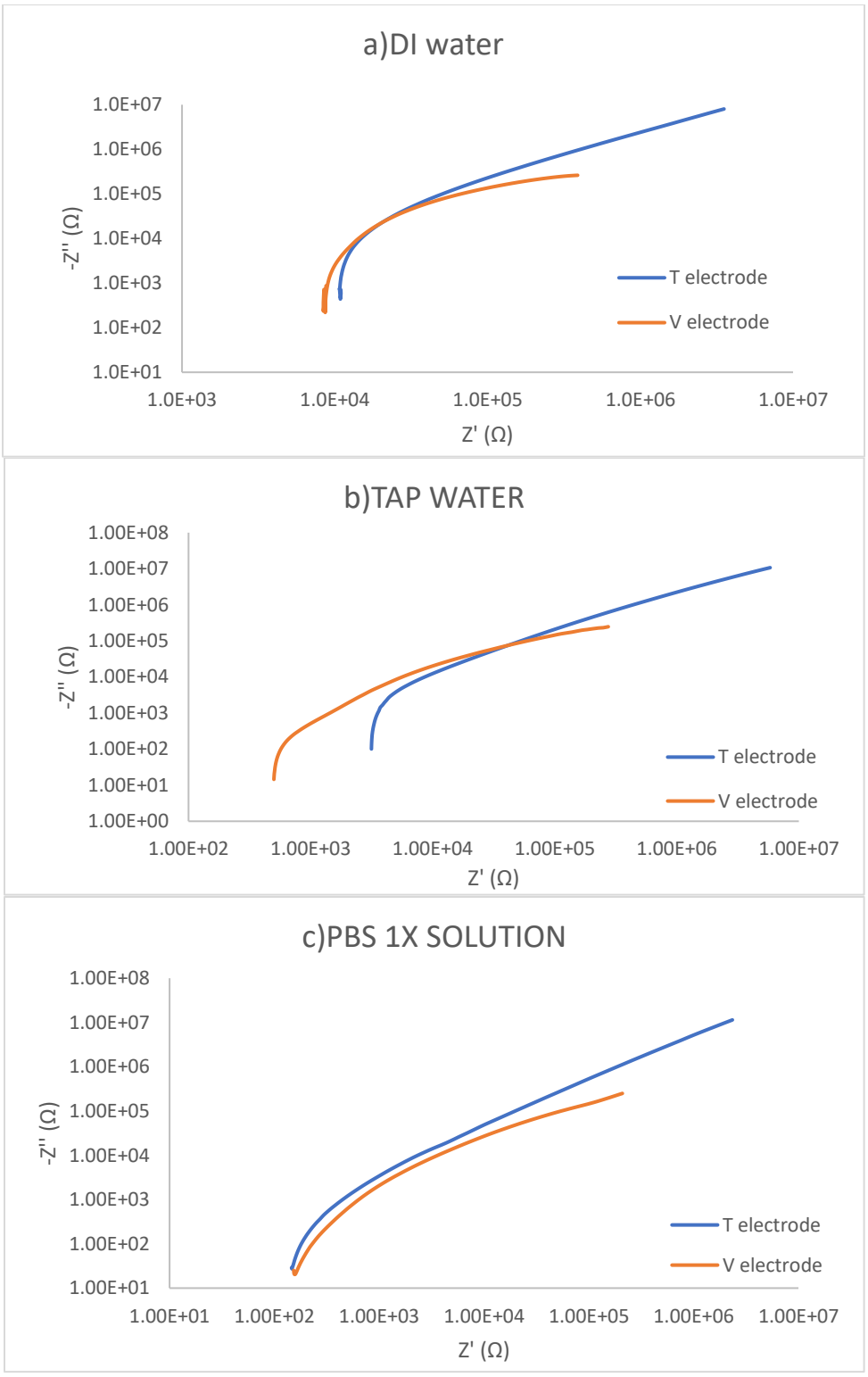

Figure 6.10: Comparison for the T and V electrode in the Nyquist plot for three different fluids (a) DI water, (b) Tap water (c) PBS 1x solution

EIS is provenience to find the statistics of area-specific impedance which can be get by multiplying the real and imaginary parts of the impedance by the electrode cross-sectional area. In figure 6.10,we can demonstrate for each liquid substaces the range of the T electrode is much higher than the V electrode. In the case of DI water and Tap water both of the graphs intersect at a certain point whereas in the PBS 1x solution it goes parallel. For the PBS (1X) solution, the imaginary value for the T electrode is always high than the V electrode, and the real part is always greater in the V electrode as the resistive nature always remains bigger in the V electrode than T. In DI water and Tap water, T and V electrodes present similar attributes where the quantity is slightly different.

Thus, from the complex spectra, the kinetics of electron transfer or the characteristics of diffusion can be extracted through analysis.

6.1.4 Subtracting results from Array Electrode Pattern

In micro or nano interfacial space, it is considered to accommodate only the interface between the solid surface and the liquid. Like any electrolyte liquid, an electrode certainly has an electric double layer (EDL) which performs as a place for local charge distribution at the interface. It is also called Debya length and acts as a capacitor in electrical measurement.

Again, the frequency dependence of the capacitance might be the result of a purely physical effect caused by the cell or the electrode geometry. That is why after T and V , the Array electrode was patterned to see the difference.

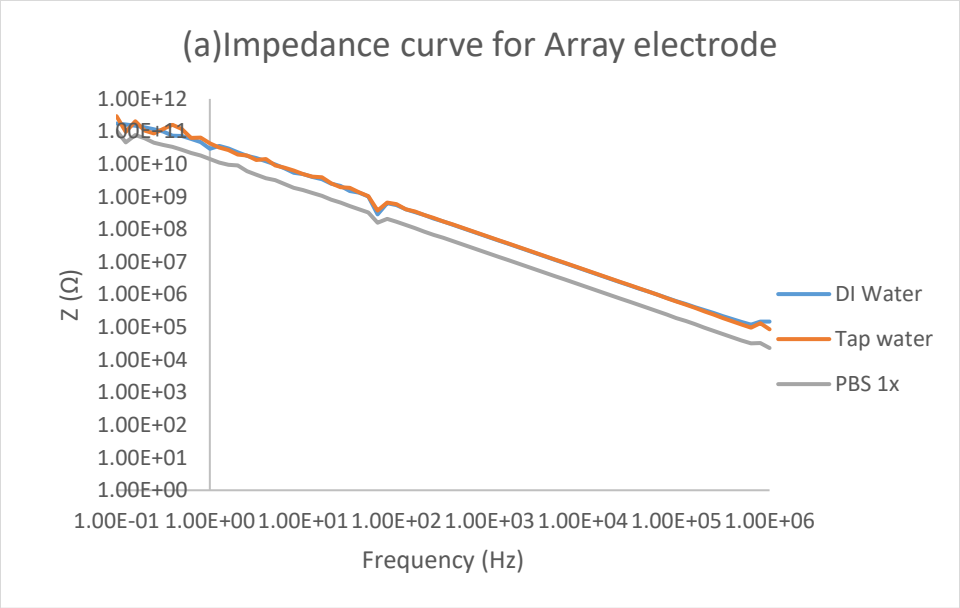

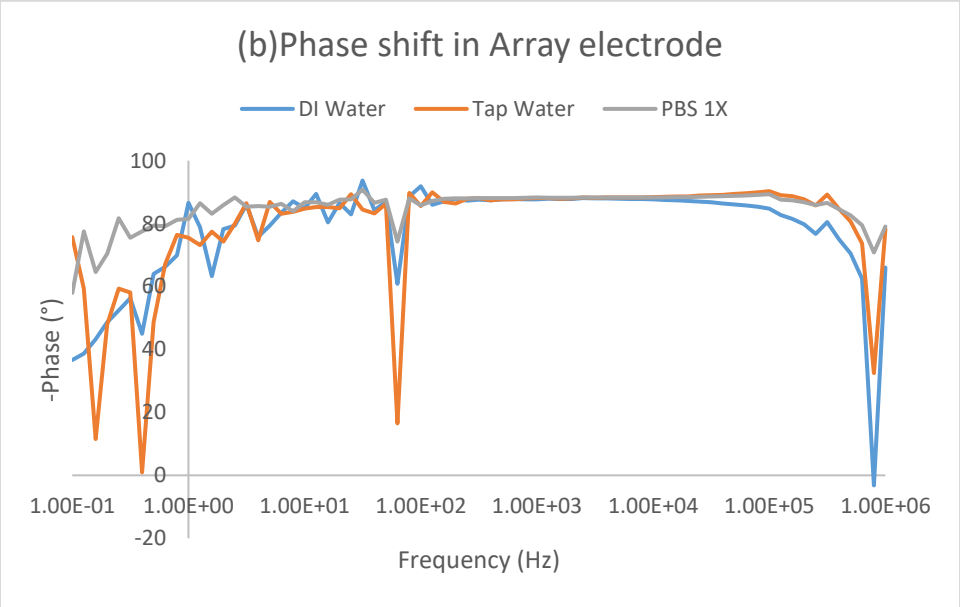

Figure 6.11: (a)Impedance Vs Frequency(b) Phase shift Vs Frequency curve for three different fluids for the Array electrodeS

In this bode plot here the difference between is much smaller than the previous results and in both phase and impedance graphs the electrolyte fluids keep linearity for longer than V and T electrodes.Still the impedance od PBS 1x is lower and in the phase shift alsoThe phase of

DI water drop first. Though the impedance and phase shift graphs shows less diversion in figure 6.11(a) it can be seen clearly in table 6.3, that it still contains the same pattern.

Table 6.3: Impedance and phase comparison chart of Array electrode

		DI water		Tap Water		PBS1x	
Index	Frequency (Hz)	Z (Ω)	-Phase (°)	Z (Ω)	-Phase (°)	Z (Ω)	-Phase (°)
1	1000000	148721.7	66.08432	86051.88	78.27861	22964.41	79.0252
2	794330	147692.2	-3.20933	133705	32.52678	32784.12	70.8391
3	630960	119541.5	62.45628	97409.8	73.64479	31800.21	79.46912
4	501190	145601.4	70.57044	120514.8	80.73362	39397.17	82.65518
5	398110	177476.4	75.02769	150851.5	84.62387	49163.12	84.5888
6	316230	218874.7	80.4775	190276.1	89.24259	61643.12	86.62574
7	251190	271880	76.76436	246321.7	85.73307	77887.94	85.86227
8	199530	332521	79.73152	308043.7	87.76148	97489.41	86.80795
9	158490	411345.1	81.52695	389456.2	88.69524	122544.4	87.37342
10	125890	512227.4	82.75099	493944.9	89.07481	154037.6	87.65658
11	100000	631801	84.80485	618264.8	90.3044	192136.4	89.29771
12	79433	787955.9	85.36725	780875.1	89.99454	241418.6	89.10314
13	63096	985011.3	85.76132	983952.3	89.67071	303136.1	88.92653
14	50119	1230006	86.13601	1236034	89.42233	380502.3	88.79156
15	39811	1535994	86.44167	1552372	89.16027	477083.1	88.68162
16	31623	1920544	86.78262	1947042	88.99471	598352.2	88.59914
17	25119	2401532	87.0358	2443652	88.90949	749685.7	88.52996
18	19953	3004607	87.15895	3062862	88.67119	938174.4	88.39134
19	15849	3764767	87.36411	3842984	88.59168	1176438	88.37655
20	12589	4717611	87.53734	4819337	88.50547	1475071	88.36294
21	10000	5911105	87.70716	6044444	88.39113	1848960	88.33898
22	7943.3	7400144	87.79207	7565438	88.3532	2318845	88.34562
23	6309.6	9274797	87.85389	9489121	88.33925	2905260	88.33259
24	5011.9	11626544	87.94377	11893798	88.31116	3643011	88.32679
25	3981.1	14568373	87.98571	14911335	88.28319	4565007	88.32493
26	3162.3	18264125	87.99687	18682739	88.26195	5723743	88.31944
27	2511.9	22891739	88.09892	23413396	88.29333	7177494	88.33586
28	1995.3	28691794	87.85144	29345043	87.96846	8996701	88.19487
29	1584.9	35966175	87.81365	36767038	87.92581	11278056	88.19397
30	1258.9	45026373	87.89078	46097797	88.07445	14144171	88.2433
31	1000	56495104	87.69358	57718148	88.0894	17710103	88.28757
32	794.33	70588712	87.73058	71889949	88.00966	22189640	88.20545
33	630.96	88521393	87.77188	90354521	87.75067	27856342	88.16029
34	501.19	1.11E+08	87.73968	1.13E+08	87.74097	34893504	88.14521

35	398.11	1.39E+08	87.43931	1.41E+08	87.44771	43658978	88.09362
36	316.23	1.74E+08	87.5851	1.77E+08	88.11308	54698754	88.10939
37	251.19	2.16E+08	87.34875	2.24E+08	87.94	68426819	88.04617
38	199.53	2.75E+08	87.93525	2.76E+08	86.34988	85788555	88.01233
39	158.49	3.37E+08	87.08145	3.5E+08	86.93235	1.08E+08	87.86959
40	125.89	4.16E+08	85.96931	4.14E+08	89.92819	1.37E+08	87.21726
41	100	5.56E+08	91.88504	5.9E+08	85.60821	1.7E+08	85.82324
42	79.433	6.37E+08	88.62608	6.64E+08	89.77111	2.08E+08	87.99552
43	63.096	2.85E+08	60.90697	3.76E+08	16.52219	1.6E+08	74.25424
44	50.119	1.03E+09	86.99442	1.05E+09	86.29897	3.29E+08	87.66094
45	39.811	1.33E+09	84.20882	1.36E+09	83.24117	4.12E+08	86.5973
46	31.623	1.49E+09	93.70541	1.87E+09	84.46114	5.14E+08	90.79109
47	25.119	2.14E+09	82.91511	1.95E+09	89.37415	6.57E+08	87.69156
48	19.953	2.53E+09	86.60417	2.6E+09	84.87123	8.1E+08	87.58331
49	15.849	3.43E+09	80.38893	3.93E+09	85.23552	1.06E+09	85.95237
50	12.589	4.01E+09	89.47046	4.18E+09	85.3128	1.3E+09	86.77695
51	10	4.9E+09	84.89445	4.96E+09	84.7448	1.59E+09	86.79375
52	7.9433	5.48E+09	87.08564	6.35E+09	83.78786	1.87E+09	83.94125
53	6.3096	7.52E+09	83.45923	7.85E+09	83.14887	2.47E+09	86.30234
54	5.0119	9.73E+09	79.34319	9.13E+09	86.8601	3.19E+09	85.38057
55	3.9811	1.21E+10	75.86208	1.43E+10	74.73158	3.68E+09	85.53847
56	3.1623	1.54E+10	85.94275	1.33E+10	86.45843	4.75E+09	85.40859
57	2.5119	1.79E+10	79.41195	1.82E+10	79.97301	6.01E+09	88.3695
58	1.9953	2.28E+10	78.23769	1.97E+10	74.31011	9.16E+09	85.88217
59	1.5849	3.02E+10	63.2714	2.68E+10	77.4214	9.46E+09	83.17397
60	1.2589	3.61E+10	78.90201	3.23E+10	73.20549	1.13E+10	86.48282
61	1	2.95E+10	86.62057	4.35E+10	75.5461	1.44E+10	81.5577
62	0.79433	4.76E+10	69.93374	6.51E+10	76.37882	1.82E+10	81.2058
63	0.63096	5.91E+10	66.23398	6.42E+10	67.01695	2.21E+10	79.1542
64	0.50119	7.21E+10	64.06585	1.21E+11	48.65124	2.74E+10	79.35945
65	0.39811	7.4E+10	45.04256	1.61E+11	0.947913	3.37E+10	77.52347
66	0.31623	9.96E+10	56.33557	1.2E+11	58.11717	3.87E+10	75.47966
67	0.25119	1.16E+11	52.46467	8.76E+10	59.34288	4.53E+10	81.73835
68	0.19953	1.33E+11	48.6952	1.08E+11	47.93026	6.19E+10	70.37499
69	0.15849	1.51E+11	43.29241	2.05E+11	11.48813	7.8E+10	64.66468
70	0.12589	1.65E+11	38.682	9.81E+10	59.37766	4.66E+10	77.55109
71	0.1	1.77E+11	36.61387	2.96E+11	75.66331	1.07E+11	57.983

Normally double-layer capacitance is a frequency-dependent feature which often approximated by a CPE. However, this empirical component gives the little amount of information on the physical origin of the dispersion. For this electrode arrangement the

capacitive nature sustains the highest and longest in the higher region of frequencies. From almost 100Hz to the 0.1MHz it showed resistive nature strong than capacitive nature.

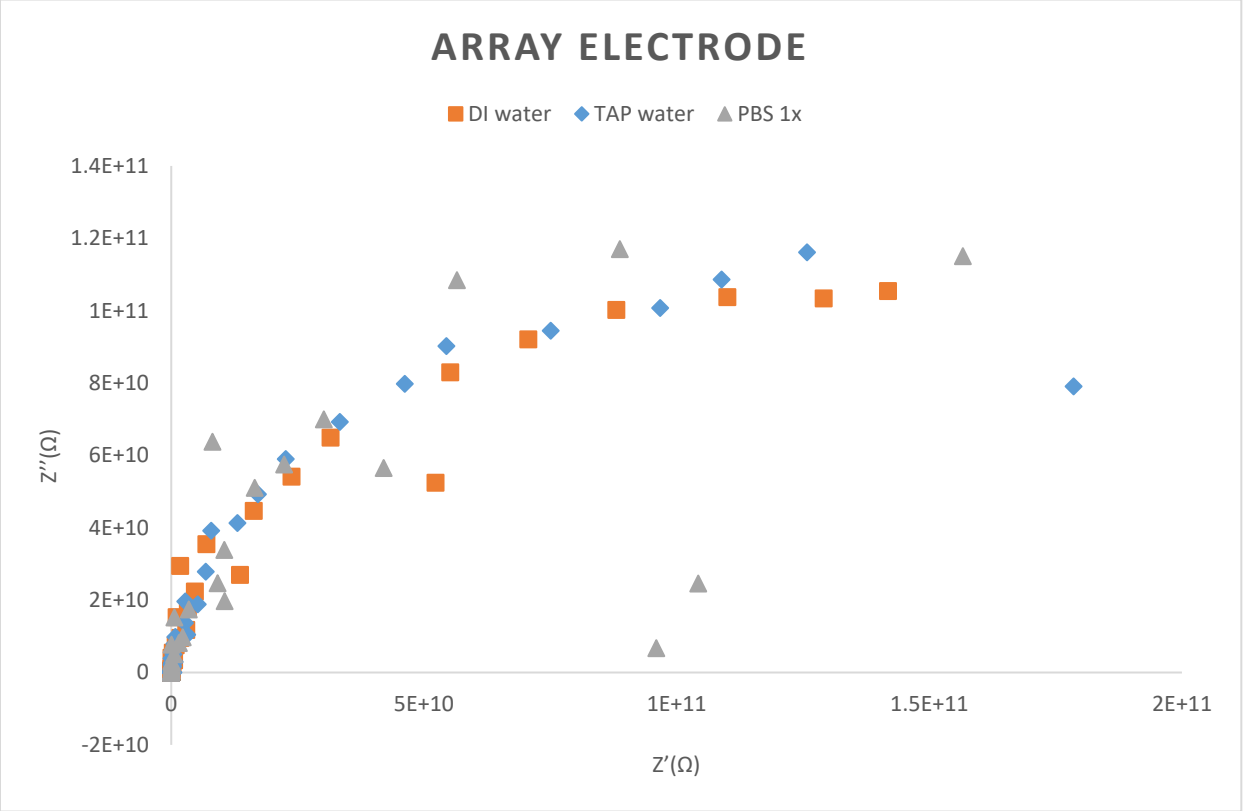

Figure 6.12: Schematic Faradaic impedance spectra, which are presented in the form of the Nyquist plot for three different fluids in the Array-shaped electrode

In the case of the Nyquist plot of Array electrode, it showed some scattered points rather than the fully continuous value that is why it is plotted in dots for better understanding in figure 6.12. All three of them showed the characteristics of a modified electrode where most of the part of the impedance is controlled by interfacial electron transfer because of its half-circle nature. Therefore, in this pattern, all conductivity ranges can be used where it's needed to slow electron transfer in the definite frequency range. Generally, the plot becomes a semicircle, which presents

a charge transfer process, and the charge transfer amount is signified by the size of the semicircle.

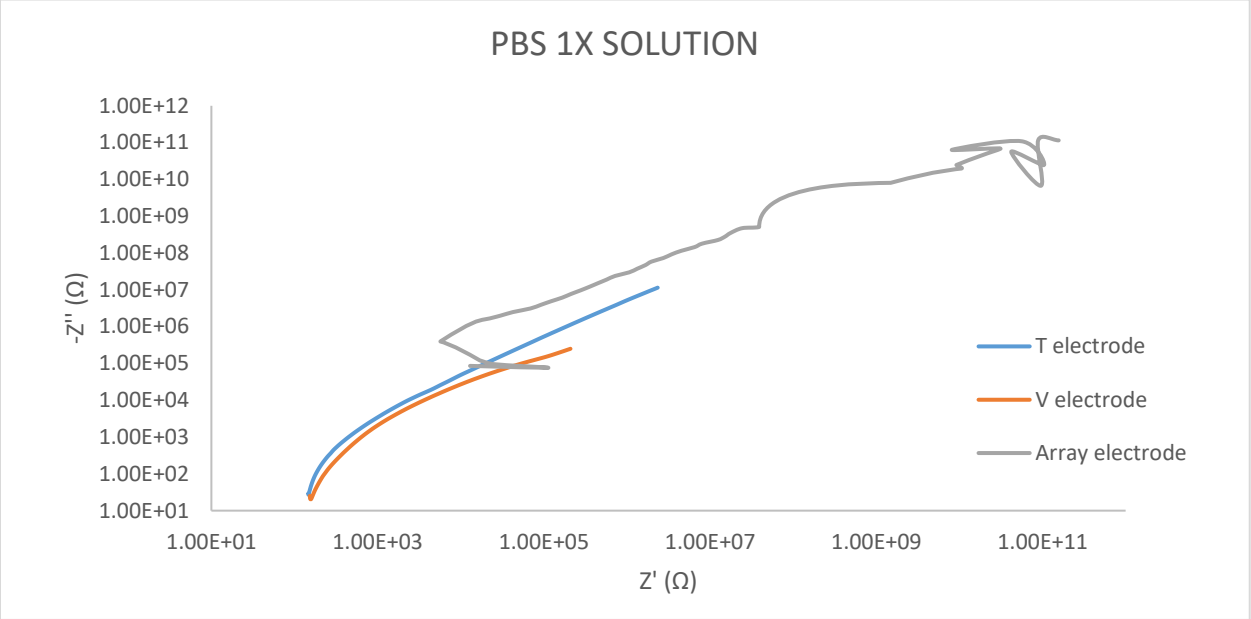

Figure 6.13: Comparative graph of T, V, and Array Electrode in PBS 1X Solution

In the comparison of V and T electrodes, a wide range of impedance is found in the Array electrode in the same range of frequency. It can be used on those sensitive applications which need a higher range of impedance.

This microfluidic channel can be beneficial in biotechnology. As a homogenous biosensing substrate, microfluidic liquid interfaces have been used for quantitative molecular detection and kinetic analysis in the solution phase. The interface is produced with the help of laminar flow, where two streams combine at a fluidic junction and proceed side-by-side down the main channel.

6.2 Particle manipulation in Micro-PIV

Various particle manipulation experiment was held for T and V electrode before which was given in Parvez MS et al. and Guillermo et al. Multiple experiments were performed to find the flow of the bioparticles across array microelectrode system to provide the necessary data for find it application. Here, the particle manipulation range for array electrode is demonstrated by varying different content. The Eclipse LV100 microscope was used at 10x magnification in 100 frames to take the real-time images to analysis. All the experiment was done by DI water with the mix of

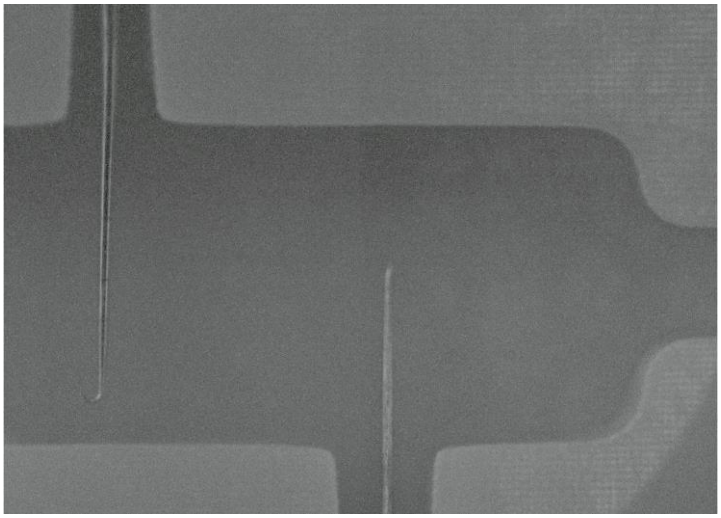

Figure 6.14 : Microscopic view of a part of the microchannel of Array electrode pattern

As there are eight electrodes in the array pattern it is not possible to focus all of them together in the microscope. Thereupon only 1 electrode is focused to get a clear picture of the particle movement. To see the best range the experience was focused on both ACEO and ACET range. By regulating the amplitude and frequency of AC signals, diverse directed surface flows are produced on electrodes to regulate and transport particles.

As AC electroosmosis (ACEO) is mainly dependent on the formation of an electric double layer (EDL) at the interface when the voltage increase it gets to ACET from ACEO. Particle movement is hard to find in low voltage. That is why mainly ACET is used in biological particle movement instead of ACEO. But for the Array design each of the pair electrodes even the movement is small it can manipulate particles and can directed according to the different application of microfluidics.

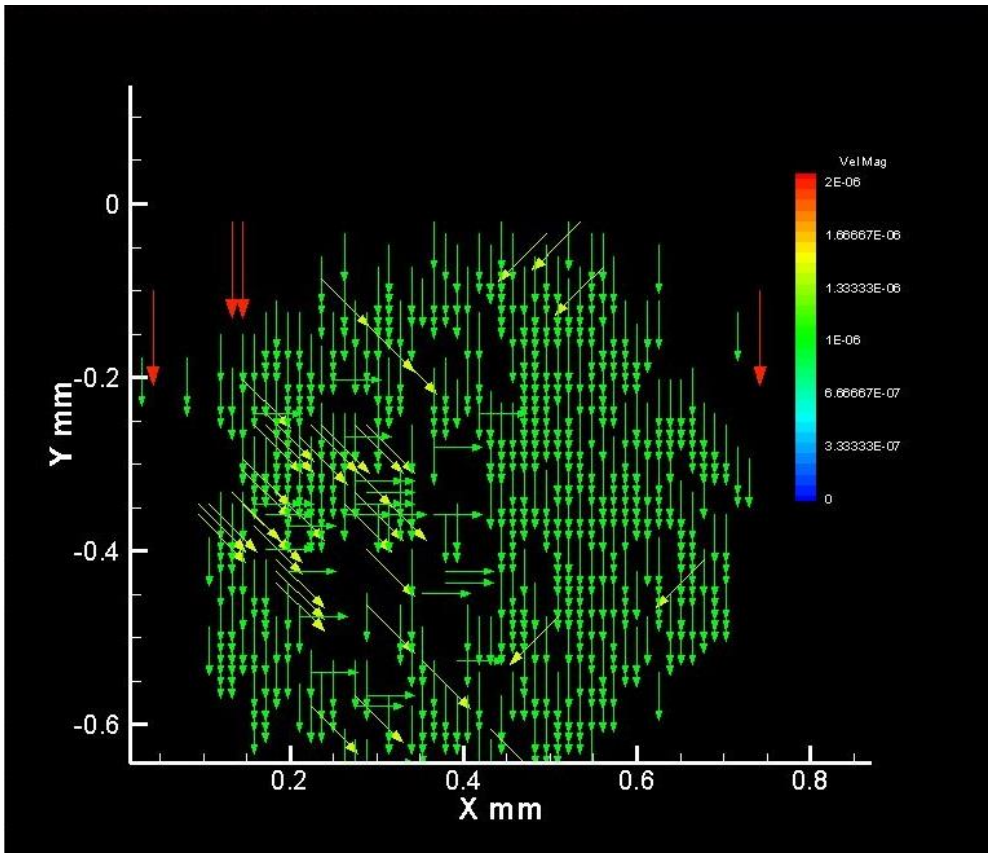

Figure 6.15: Particle flow in array electrode in 6V AC supply and 1KHz frequency range

Comparatively, in low voltage (4V to 8V) and frequency (1kHz to 5kHz), the particle seems to move, and the velocity is also in the medium range but didn't form any vortex.

When excited with the AC signal, ACET the effect would create vortices that will give active guidance of particles to be trapped at the oval region between the orthogonal electrodes. ACET appears from the interaction of a temperature gradient in the bulk of the liquid substances and a non-uniform AC electric field. In the range of 10V to 15V and with the frequency range of above 100KHz the particle manipulation seems in one particular direction even in the static fluids and it can be used for a particular flow in figure 6.15.

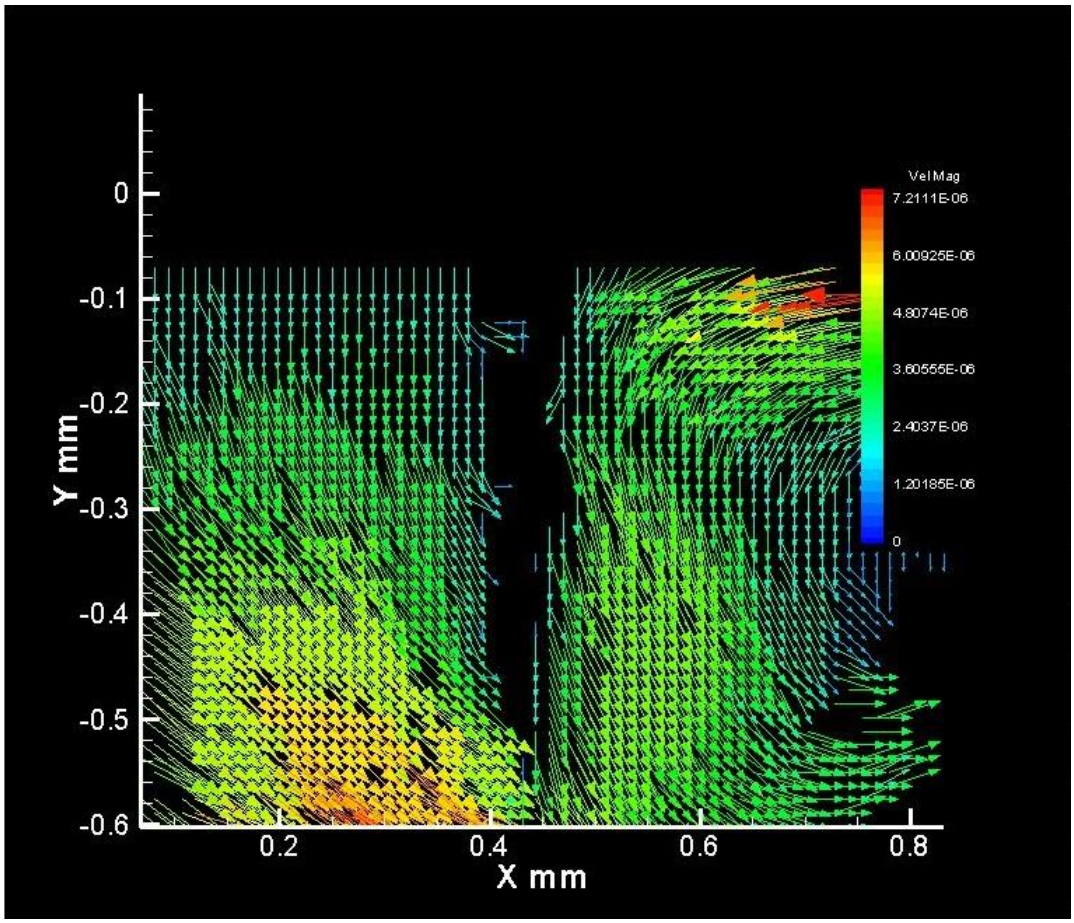

Figure 6.16: Particle flow in array electrode in 11V AC supply and KHz frequency range

As array pattern has total eight electrodes its possible to get particle manipulation easily in the each step even they are connected to each other. With this pattern it can be also used with different souces at the same time to get a better result if needed. Two prime ACEK mechanisms,

the ACEO and the ACET, can incite microfluidic motion in a microfluidic channel with a definite type of electrode pattern. Micro-flow and its patterns change with applied voltage, frequency as well as electrode pattern. ACEO originates fluid motion by actuating mobile charges in the double layers when ACET happens for the interaction of a temperature gradient in the bulk of the electrolytes and a non-uniform AC electric field. Both ACEO and ACET velocities have different dependencies and applied field in particle manipulation.

CHAPTER VII

CONCLUSIONS AND FUTURE WORK

7.1 Conclusion

Electrochemical impedance spectroscopy (EIS) measurements allow the characterization of different patterns with different electrical or structural properties. Impedance spectrum not only simply shows the sum of the solution resistance and interfacial impedance, but they also coupled somehow the resultant. Here we compare two different patterns of the electrode (T and V) and three different kinds of fluids (DI water, tap water and PBS) of different conductivity and observe their behavior in both bode plots and Nyquist plots. It was seen that V electrodes showed less capacitive characteristics than T electrodes. Moreover, in both electrodes' electrolyte fluids, periodic characteristics and the impedance get high with the decrease of conductivity and frequency. However, the T electrode showed a very higher impedance. In the later part, a different arrangement of electrodes is prototyped by a 3D printing microchannel, which is called array pattern electrode and was run the experiments for the same three fluids for different conductivity. Array electrode patterns exhibit a large range of impedance variance for the same frequency, which can be used where a small impedance variation is needed. Array electrode particularly showed impedance pattern caused by interfacial electron transfer, which has another group of applications in the biotechnology for slow electron transfer. By using the information about characterizing the electrode interface, we can choose the operating region to

do our microfluidics experiments. For AC electrokinetic behavior we need to define all the AC electroosmosis (ACEO), AC electrothermal (ACET) and DEP regions. As we experiment large band of frequency, it both covers ACEO and ACET application. These experiments put a lower frequency region for the ACEO experiments and higher frequency regions for ACET applications.

The Micro-PIV microflow was investigated by AC electrokinetic on another array microelectrode configuration pattern. Various experiments were performed in order to obtain the desired microflow during this research work. These procedures help to determine the proper mechanism to manipulate the particles by selecting an appropriate signal frequency and voltage. With the help of multiple electrodes in array pattern it can be proven a better particle manipulator. After shifting the particles to the detection area or stagnation area by ACEO and ACET effects, the DEP method can be applied as a trapping force to capture the particles as a holding mechanism. The designed pre-concentrator is non-mechanical and makes it more reliable than the mechanical device that needs moving parts, which are subjected to failure. It also uses the latest 3D printing technology for which no costly cleanroom is needed, which makes it more user-friendly. These results can also be useful in various applicable fields like fuel cell development, as applied immunosensor or other biosensors, monitoring biofilm development, and bacterial interaction with electrodes.

7.2 Future Works

Some experiments already processing and proposed for the future work of this thesis works. Besides, using a 3D printed microfluid channel to analyze the microflow can also use to create a mold for Polydimethylsiloxane (PDMS) channel, which is widely used in

biotechnology. Generally, PDMS channels are made in bioprinting but with this one, it is possible to make PDMS channels at a low cost.

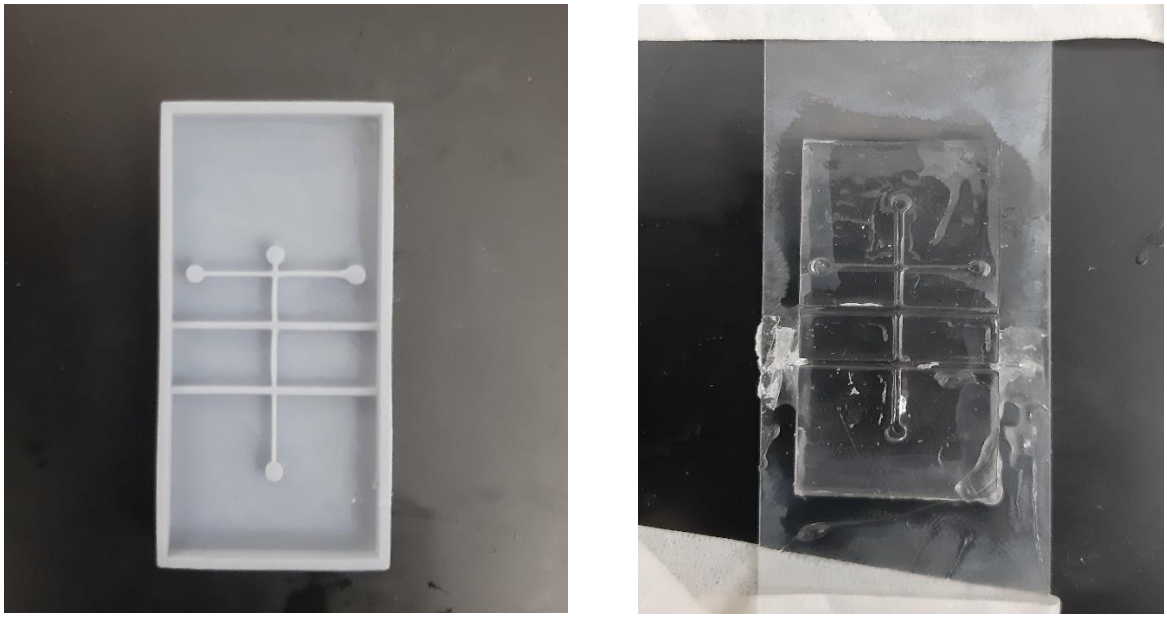

Figure 7.1: 3D printed mold for the microchannel(left) cured PDMS channel made from this mold(right)

Also, other different electrolytes can be used in this experiments and can make some connections between EIS and Micro-PIV data for the practical use of the microflow in biotechnology some bioparticle will be use for this experiment. Specially EIS is greatly effective in antigen-antibody reaction and also can be used as an immunosensor that use impedance measurements for the transduction of antigen-antibody complex formation on electronic transducers if properly used.Using EIS, amplified detection of the analyte DNA can be achieved by the coupling of functionalized liposomes or by the involvement of biocatalytic conjugates to the sensing interface providing biocatalyzed precipitation of an insoluble product on the electrodes.

REFERENCES

Barsoukov E, Macdonald J.R. , "Impedance Spectroscopy Theory, Experiment, and Applications" pp-17-21, Third Edition, First published:25 March 2018.

Bhatt KH, Grego S, Velev OD: 'An AC electrokinetic technique for collection and concentration of particles and cells on patterned electrodes', Langmuir, 21, pp. 6603–6612, 2005

Bonora PL, Defloriana F, Fedrizzi L, "Electrochemical Impedance Spectroscopy As A Tool For Investigating Underpaint Corrosion", Volume 41, Issues 7–8, May–June 1996, Pages 1073-1082

Cole KS, Cole RH: "Dispersion and absorption in dielectrics II.Direct current characteristics" J Chem Phys 1942, 10 :98–105

Green NG, Ramos A, Gonzalez A, et al.: 'Fluid flow induced by nonuniform ac electric fields in electrolytes on microelectrodes. I. Experimental measurements', Phys. Rev. E, 61, pp. 4011–18, 2000

Green NG, Ramos A, Gonzalez A, et al.: 'Fluid flow induced by nonuniform ac electric fields in electrolytes on microelectrodes. III. Observation of streamlines and numerical simulation', Phys. Rev. E, 66, p. 026305, 2002

Guduru R,Uddin M, and Islam N, "Optimization of An Electrokinetic Orthogonal Electrode Pattern for Multifunctional System", IMECE 2016

Islam N, Lian M, Wu J: 'Enhancing cantilever capability with Integrated AC Electrokinetic Trapping Mechanism', J. Microfluid. Nanofluid, 3, (3), pp. 369–375, 2007

Katz E, Willner I, "Probing Biomolecular Interactions at Conductive and Semiconductive Surfaces by Impedance Spectroscopy: Routes to Impedimetric Immunosensors, DNA-Sensors, and Enzyme Biosensors", Electroanalysis 2003, 15, No. 11

Lian M., Islam N and Wu J. "AC electrothermal manipulation of conductive fluids and particles for lab-chip applications" IET Nanobiotechnology, 1, (3), pp. 36–43, 2007

Parvez M.S, Rubby M.F, Iqbal S, Islam N, "Dc-Biased Ac Electrokinetics Effect On V-Shaped Electrode Patterns for Microfluidics Applications", IMECE 2019

Pethig R : 'Application of A.C.: electrical fields to themanipulation and characterisation of cells' in Karube I(Ed.): 'Automation in Biotechnology',pp. 159–185(Elsevier, 1991)

Salari A, Navi M, Lijnse T and Dalton C "AC Electrothermal Effect in Microfluidics: A Review", 10, 762, Micromachines 2019

Wu J, "Interactions of Electrical Fields with Fluids: Laboratory-on-a-chip Applications," IET Nanobiotechnology, 2(1), pp. 14-27,2008.

Zhen H., Florian M, "Exploring the use of electrochemical impedance spectroscopy (EIS) in microbial fuel cell studies" Energy Environ. Sci., 2, 215-219, 2009

Zia A.I., Syaifudin A.R.M, et al. "Electrochemical impedance spectroscopy based MEMS sensors for phthalates detection in water and juices" J. Phys.: Conf. Ser. 439 012026, (2013).

BIOGRAPHICAL SKETCH

Shanzida Kabir was born in Dhaka in 1996. Being blessed with an engineering family, her enthusiasm for this subject started from my home from an early age. Family inspiration as well as her own fascination inspired her to become an engineer.

With an aim to be a part of the engineering committee, she undertook her undergraduate degree in Electrical Electronics and Communication Engineering (EECE) from Military Institute of Science and Technology (MIST), Bangladesh, and then did her Master's at The University of Texas Rio Grande Valley (UTRGV) in Electrical engineering. She published some of her research work in IEEE and ASME conferences and reviewed some articles. Apart from having academic proficiency, she has participated actively in many extracurricular activities like cultural, social service events, and sports. Her research interest mainly focused on microfluidic devices used in lab-on-a-chip and biotechnology applications. After graduating, Shanzida Kabir is actively looking forward to joining the industrial field to apply engineering knowledge in a more structured corporate environment.

permanent email: kabir.shanzida23@gmail.com